

**NOAA NESDIS  
CENTER FOR SATELLITE APPLICATIONS  
AND RESEARCH**

**Vegetation Index (VI) Product**

**ALGORITHM THEORETICAL  
BASIS DOCUMENT**

**Version 1.0**

AUTHORS:

# NOAA NESDIS STAR

ALGORITHM THEORETICAL BASIS DOCUMENT

Version: 1.0

Date: Feb. 2, 2018

TITLE: VIIRS VI Algorithm Theoretical Basis Document

Page 2 of 64

---

Zhangyan Jiang (IMSG)

Yunyue Yu (STAR)

Mingshi Chen (IMSG)

Feng Zhao (IMSG)

Ivan Csiszar (STAR)

## VI ALGORITHM THEORETICAL BASIS DOCUMENT VERSION HISTORY SUMMARY

Version	Description	Revised Sections	Date
1.0	New document creation	New Document	2/1/2018

## TABLE OF CONTENTS

	<u>Page</u>
<b>LIST OF FIGURES</b> .....	<b>5</b>
<b>LIST OF TABLES</b> .....	<b>6</b>
<b>LIST OF ACRONYMS</b> .....	<b>7</b>
<b>ABSTRACT</b> .....	<b>9</b>
<b>1. INTRODUCTION</b> .....	<b>10</b>
1.1 PURPOSE OF THIS DOCUMENT .....	11
1.2 WHO SHOULD USE THIS DOCUMENT .....	11
1.3 INSIDE EACH SECTION .....	11
<b>2. VIIRS VI PRODUCTS OVERVIEW</b> .....	<b>13</b>
2.2 INSTRUMENT CHARACTERISTICS .....	14
<b>3. ALGORITHM DESCRIPTION</b> .....	<b>15</b>
3.1 PROCESSING OUTLINE .....	15
3.2 ALGORITHM INPUT .....	18
3.2.1 <i>VIIRS surface reflectance data</i> .....	18
3.2.2 <i>VIIRS TOA reflectance I1 data</i> .....	18
3.2.3 <i>VIIRS TOA reflectance I2 data</i> .....	19
3.2.4 <i>VIIRS geolocation data</i> .....	19
3.2.5 <i>VIIRS Aerosol Optical Depth (AOD) data</i> .....	19
3.2.6 <i>VIIRS cloud mask</i> .....	19
3.2.7 <i>MODIS land/water mask</i> .....	19
3.3 THEORETICAL DESCRIPTION .....	19
3.3.1 <i>Gridding</i> .....	21
3.3.2 <i>Compositing</i> .....	21
3.3.3 <i>Reflectance aggregation</i> .....	27
3.3.4 <i>VI calculation</i> .....	27
3.3.5 <i>VI QA assignment</i> .....	28
3.4 ALGORITHM OUTPUT .....	39
3.5 PRACTICAL CONSIDERATIONS .....	46
3.5.1 <i>Numerical computation consideration</i> .....	46
3.5.2 <i>Programming and procedural consideration</i> .....	46

# NOAA NESDIS STAR

## ALGORITHM THEORETICAL BASIS DOCUMENT

Version: 1.0

Date: Feb. 2, 2018

TITLE: VIIRS VI Algorithm Theoretical Basis Document

Page 4 of 64

---

3.5.3	<i>Quality assessment and diagnostics</i> .....	47
3.5.4	<i>Exception handling</i> .....	47
3.6	SAMPLE RESULTS.....	47
3.7	VALIDATION EFFORTS .....	50
3.7.1	<i>Validation strategy</i> .....	50
3.7.2	<i>Validation of VIIRS VI EDR granule product</i> .....	51
3.7.3	<i>Validation of VIIRS gridded and composited VI products</i> .....	55
<b>4.</b>	<b>ASSUMPTIONS AND LIMITATIONS</b> .....	<b>59</b>
4.1	ASSUMPTIONS .....	59
4.2	LIMITATIONS .....	59
<b>5.</b>	<b>LIST OF REFERENCES</b> .....	<b>60</b>

## LIST OF FIGURES

	<u>Page</u>
Figure 1. Flow chart of VIIRS VI system.....	17
Figure 2. Yearly mean sensor zenith angles and yearly mean percentage of forward scatter direction pixels of the maximum SAVI composited images over the tile H10V05 in 2007 as functions of the soil adjustment factor (L) values.....	22
Figure 3. Mean EVI composited by the maximum SAVI method using the five soil adjustment factor (L) values over the tile H10V05 in 2007.....	23
Figure 4. Histograms of the sensor zenith angles composited by the traditional MVC based on NDVI (L=0) (a) and by the MVC based on SAVI (L=0.05) in different seasons (compositing periods beginning at DOYs 041, 121, 217 and 313) in 2007 over the tile H10V05.....	24
Figure 5. C is designed as a function of the maximum SAVI.....	25
Figure 6. Comparison of the maximum value compositing and the maximum view angle adjusted SAVI compositing.....	26
Figure 7. Histograms of sensor zenith angles composited by the MVA-SAVI method at different seasons. ....	26
Figure 8. Data fields of the VIIRS daily global VI product.....	42
Figure 9. VIIRS VI browse images in the week of Oct 5-20, 2017. (a) VIIRS TOC global 0.036° 16-day composite EVI; (b) VIIRS TOC regional 0.009° 16-day composite EVI; (c) VIIRS TOA global 0.036° 16-day composite NDVI; (d) VIIRS TOA regional 0.009° 16-day composite NDVI; (e) VIIRS TOC global 0.036° 16-day composite NDVI; (f) VIIRS TOC regional 0.009° 16-day composite NDVI.....	50
Figure 10. VIIRS TOA NDVI, TOC EVI and TOC NDVI Accuracy, Precision and Uncertainty (APU) are plotted as function of VIIRS VI values in global inter-comparison with MODIS VI. ....	52
Figure 11. VIIRS TOA NDVI, TOC EVI and TOC NDVI Accuracy, Precision and Uncertainty (APU) time series in global inter-comparison with MODIS VI. ....	54
Figure 12. The EOS Land Validation Core Sites of FLUXNET are intended as a focus for land product validation over a range of biome types. ....	56
Figure 13. Scatterplots of the VIIRS and MODIS 16-day composite TOA NDVI data, over the 35 FLUXNET sites, on the Julian Day 297 (top-left) and Julian Day 313 (bottom-left), and the TOC EVI data on the Julian Day 313 (top-right) and Julian Day 313 (bottom-right).....	57
Figure 14. Bar-chart of the VIIRS and MODIS VI comparisons over 6 sample FLUXNET sites, in which the left 3 sites show great consistency of the two products (i.e. VIIRS VIs and MODIS VIs), while the right 3 sites show some obvious differences. ....	58

## LIST OF TABLES

	<u>Page</u>
Table 1. Requirement of JPSS Vegetation Indices Product .....	13
Table 2. Summary of VIIRS VNIR and SWIR Spectral Band Characteristics.....	14
Table 3. Input Data of the VIIRS VI System .....	18
Table 4. QF1 Surface Reflectance .....	28
Table 5. QF2 Surface Reflectance .....	29
Table 6. QF3 Surface Reflectance .....	30
Table 7. QF4 Surface Reflectance .....	31
Table 8. QF5 Surface Reflectance .....	32
Table 9. QF6 Surface Reflectance .....	33
Table 10. QF7 Surface Reflectance .....	34
Table 11. Bit Layout of the Four QFs in the NVPS VI Product .....	37
Table 12. VIIRS VI Output Files .....	40
Table 13. VIIRS VI Output Files Standard Name Description .....	41
Table 14. Data Fields of the NVPS VI Product.....	43
Table 15. Meta Information of the NVPS VI Product .....	44
Table 16. VIIRS VI EDR global APU estimation.....	54
Table 17. VIIRS VI EDR global APU estimation in comparison with MODIS VIs .....	55
Table 18. VIIRS VI Validation Statistics.....	58

## LIST OF ACRONYMS

ARVI	Atmospheric Resistant Vegetation Index
ATBD	Algorithm Theoretical Basis Document
CDR	Critical Design Review
DoD	Department of Defense
EVI	Enhanced Vegetation Index
GVF	Green Vegetation Fraction
GVFP	Green Vegetation Fraction Product
GVPS	Global Vegetation Processing System
HDF	Hierarchical Data Format
IMSG	I. M. Systems Group
IP	Intermediate Product
JPSS	Joint Polar Satellite System Program
LAI	Leaf Area Index
L1RDS	Level 1 Requirements Supplement
NIR	Near Infrared
km	Kilometer
MB	Mega Byte
μm	Micron
MODIS	Moderate Resolution Imaging Spectroradiometer
MVC	Maximum Value Compositing
NASA	National Aeronautics and Space Administration
NCEP	National Center for Environmental Prediction
NDVI	Normalized Difference Vegetation Index
NESDIS	National Environmental Satellite, Data, and Information Service
NetCDF	Network Common Data Form
NIR	Near Infrared
NOAA	National Oceanic and Atmospheric Administration
OSPO	Office of Satellite and Product Operations
PDR	Preliminary Design Review
PNG	Portable Network Graphics
QA	Quality Assurance
RIP	Retained Intermediate Product
SAVI	Soil Adjusted Vegetation Index
SEVIRI	Spinning Enhanced Visible and Infrared Imager
SNPP	Suomi National Polar-orbiting Partnership

# NOAA NESDIS STAR

ALGORITHM THEORETICAL BASIS DOCUMENT

Version: 1.0

Date: Feb. 2, 2018

TITLE: VIIRS VI Algorithm Theoretical Basis Document

Page 8 of 64

---

SPSRB	Satellite Products and Services Review Board
STAR	Center for Satellite Applications and Research
TIFF	Tagged Image File Format
TOA	Top of Atmosphere
TOC	Top of Canopy
USGS	United States Geological Survey
VHP	Vegetation Health Product
VIIRS	Visible Infrared Imager Radiometer Suite

## ABSTRACT

This document is the Algorithm Theoretical Basis Document (ATBD) for the VIIRS Vegetation Index (VI) operational product system, developed by the NOAA/NESDIS Center for Satellite Applications and Research (STAR). The main function of the VI system is to produce Top of Atmosphere (TOA) Normalized Difference Vegetation Index (NDVI), Top of Canopy (TOC) NDVI and Enhanced Vegetation Index (EVI) from the Visible Infrared Imager Radiometer Suite (VIIRS) sensor onboard Suomi National Polar-orbiting Partnership (SNPP) satellite, for applications in numerical weather and seasonal climate prediction models at the National Centers for Environmental Prediction (NCEP). The retrieval algorithm uses VIIRS red (I1), near-infrared (I2) and blue (M3) bands centered at 0.640  $\mu\text{m}$ , 0.865  $\mu\text{m}$  and 0.490  $\mu\text{m}$ , respectively, to calculate NDVI and EVI. This document describes the details of the VI algorithm that is used for VIIRS VI production. To meet the data needs of NCEP and other potential users, the VIIRS VI algorithm produces TOA NDVI, TOC NDVI and EVI in daily, daily rolling weekly composite and 16-day composite at 4-km resolution (global scale) and 1-km resolution (regional scale). Details of these products are presented in Sections 2 and 3 of this document. Some operational considerations are given in Section 4.

## 1. INTRODUCTION

Vegetation Index (VI) is a robust empirical measure of vegetation activity at the land surface, and has been widely used to study the spatial and temporal pattern of vegetation conditions at large scale with the objective to understand the role of terrestrial vegetation in regional and global processes, such as global carbon and nitrogen cycle, global hydrological cycle and global energy cycle. The MODerate Resolution Imaging Spectrometer (MODIS) Vegetation Indices (VIs) product represented the best available data source for studying large scale land surface vegetation dynamics in the last two decades.

On the heritage of the NOAA AVHRR and NASA EOS MODIS, the Visible Infrared Imager Radiometer Suite (VIIRS) onboard NASA's Suomi National Polar-orbiting Partnership (S-NPP) satellite instrument was successfully launched in Nov 21, 2011. The Suomi NPP VIIRS Vegetation Index Environment Data Record (VIIRS VI-EDR) product, built and expanded on MODIS VI product, has become operational within the Suomi NPP Data Exploitation (NDE) production facility as of February 12, 2015. The NDE is a production facility within the NOAA Environmental Satellite Processing Center (ESPC), which in turn is an element of the JPSS common ground segment.

The current version of S-NPP VIIRS Vegetation Index (VI) produces gridded VI product at global scale and North America-centric regional scale. The global gridded VI products are consistent with the already operational SNPP VIIRS Green Vegetation Fraction (GVF) product gridded at 4 km resolution. Meanwhile the North America-centric regional VI products, spanning from 7.5°S northward to the Pole, and from 130°E eastward to 30°E, are produced at 1 km resolution.

Three VI products are made both globally and regionally over land regions: the Top of the Atmosphere (TOA) Normalized Difference Vegetation Index (NDVI), the Top of the Canopy (TOC) NDVI, the TOC Enhanced Vegetation Index (EVI) and relevant quality flags (i.e., Land/water mask, cloud confidence, aerosol loadings and exclusion conditions). Meanwhile, quality assurances (QA) of the VI products are generated to consider impact of various environmental factors (e.g., cloudy, sun glint, aerosol). These VI products are produced at temporal scales of daily, weekly and bi-weekly at spatial resolutions with sizes of 4 km (0.036°, global scale) and 1km (0.009°, regional scale).

The algorithm development was initiated by Dr. Marco Vargas, with scientists and developers of STAR VI team, late was led by Dr. Yunyue Yu. The Office of Satellite and Product

Operations (OSPO) are responsible for product data storage, accessibility and dissemination.

### ***1.1 Purpose of This Document***

The purpose of this document is to provide a detailed description of the algorithm employed to produce the VIIRS VI product. Specifically, the document introduces the inputs required to produce the VIIRS VI product and outputs of VIIRS VI products, including TOA NDVI, TOC NDVI and TOC EVI, and also quality flags associated with these three VIIRS VI products.

### ***1.2 Who Should Use This Document***

The intended users of this document are project managers, product customers, product users, requirement reviewers and code reviewers.

Project managers, requirements reviewers and customers will use this document to determine that the desired products will be produced such that they match the specifications stated in the project requirements. Code reviewers and testers can follow the steps outlined below for conducting their tests.

Product customers will use this document to better understand the VIIRS VI products, and to learn how to use the VIIRS VI products in an appropriate manner. Product customers may come from government agencies (e.g., NOAA/NESDIS, USGS EROS), scientific communities (e.g., Universities) or remote sensing industries.

This document was prepared by the STAR JPSS/VIIRS VI development team led by Dr. Yunyue Yu and in consultation with primary customers, and data users. The responsible entity for bookkeeper, accessibility and distribution of this document is the Operational Products Development Branch (OPDB) of the NESDIS Center for Satellite Applications and Research (STAR) Satellite Meteorology and Climatology Division (SMCD).

### ***1.3 Inside Each Section***

This document contains the following sections:

Section 1.0 - Introduction. Section 1 provides the purpose and intended users of the ATBD.

Section 2.0 - VI System Overview. Section 2 describes the products generated by the algorithm and the characteristics of the instruments that supply inputs to the algorithm.

Section 3.0 - Algorithm Description. Section 3 describes the algorithm, including a processing overview, input data, physical description, mathematical description, algorithm output, performance estimates, practical considerations, and validation.

Section 4.0 - Assumptions and Limitations. Section 4 states assumptions that were made in determining that the software system architecture as designed will meet the requirements, and states limitations that may impact on the system's ability to meet requirements.

Section 5.0 - List of References. Section 5 provides a list of references cited in the document.

## 2. VIIRS VI PRODUCTS OVERVIEW

### 2.1 Objectives of VIIRS Vegetation Index

The worth of an operational VIIRS VI product has already been fully proved with the heritage of the AVHRR Normalized Difference Vegetation Index (NDVI) product (e.g. Gutman, 1991; Myneni, et al., 1997a; Gutman & Ignatov, 1998; Wessels et al., 2004; Anyamba & Tucker, 2005) and MODIS NDVI and EVI products (e.g. Huete et al., 2002; Zhang et al., 2003; Huete et al., 2006; Sims et al., 2006; Lunetta et al., 2006; Jiang et al., 2008; Funk & Budde, 2009). The current NOAA-AVHRR Global Vegetation Processing System (GVPS) operationally produces daily NDVI data from AVHRR at 16 km resolution for use by NCEP/EMC. Currently, VI product are produced from NOAA-19 AVHRR. To ensure continuous provision of VI data, The Suomi NPP VIIRS Vegetation Index Environment Data Record (VIIRS VI-EDR) product has become operational within the Suomi NPP Data Exploitation (NDE) production facility as of February 12, 2015. The current version of VI products was developed to meet the requirements:

- 1) Replacement of the GVPS production;
- 2) The JPSS operational VI products are initially generated in granule level (at 375 meter resolution at nadir), which cannot be ingested into NOAA operational monitoring and decision making systems; gridded VI products are required instead;  
A global gridded VI product suite for operational use by the NOAA National Centers for Environmental Prediction (NCEP).

In general, the VI product requirements are defined by the JPSS program level 1 requirements document, as shown in Table 1.

**Table 1. Requirement of JPSS Vegetation Indices Product**

EDR Attribute	Threshold	Objective
<b>Vegetation Indices Applicable Conditions:</b>		
1. Clear, land (not ocean), daytime only		
a. Horizontal Cell Size	0.4 km	0.25 km
b. Mapping Uncertainty, 3 Sigma	4 km	1 km
c. Measurement Range		
1. NDVI <sub>TOA</sub>	-1 to +1	NS
2. EVI (1)	-1 to +1	NS
3. NDVI <sub>TOC</sub>	-1 to +1	NS
d. Measurement Accuracy - NDVI <sub>TOA</sub> (2)	0.05 NDVI units	0.03 NDVI units

e. Measurement Precision - NDVI <sub>TOA</sub> (2)	0.04 NDVI units	0.02 NDVI units
f. Measurement Accuracy - EVI (2)	0.05 NDVI units	NS
g. Measurement Precision - EVI (2)	0.04 NDVI units	NS
h. Measurement Accuracy - NDVI <sub>TOC</sub> (2)	0.05 NDVI units	NS
i. Measurement Precision - NDVI <sub>TOC</sub> (2)	0.04 NDVI units	NS
j. Refresh	At least 90% coverage of the globe every 24 hours (monthly average)	24 hrs
<b>Notes:</b> 1. EVI can produce faulty values over snow, ice, and residual clouds (EVI > 1). 2. Accuracy and precision performance will be verified and validated for an aggregated 4 km horizontal cell to provide for adequate comparability of performance across the scan.		

## 2.2 Instrument Characteristics

VIIRS is one of five instruments onboard the SNPP satellite that launched on Oct. 28, 2011. It is intended to be the product of a convergence between the Department of Defense (DoD), NOAA and the National Aeronautics and Space Administration (NASA) in the form of a single visible/infrared sensor capable of satisfying the needs of all three communities, as well as the research community beyond. As such, VIIRS will require three key attributes: high spatial resolution with controlled growth off nadir; minimal production and operational cost; and a sufficient number of spectral bands to satisfy the requirements for generating accurate operational and scientific products. Calibration is performed onboard using a solar diffuser for short wavelengths and a blackbody source and deep space view for thermal wavelengths. The nominal altitude for the SNPP satellite is 824 km. The VIIRS scan will therefore extend to 56 degrees on either side of nadir.

The positioning of the VIIRS Visible/Near Infrared (VNIR) and Short Wave Infrared (SWIR) spectral bands is summarized in table 2. There are nine moderate (M) resolution bands and three imagery (I) resolution bands in the VNIR and SWIR spectral region. The nadir resolutions for the M and I bands are 750 m and 375 m, respectively. The GVF algorithm uses the VIIRS bands I1, I2 and M3 as input data.

**Table 2. Summary of VIIRS VNIR and SWIR Spectral Band Characteristics**

Band Name	Center	Width* (microns)	Resolution (m)
M1	0.415	0.020	750

---

---

M2	0.445	0.020	750
<b>M3</b>	<b>0.490</b>	<b>0.020</b>	<b>750</b>
M4	0.555	0.020	750
<b>I1</b>	<b>0.640</b>	<b>0.075</b>	<b>375</b>
M5	0.673	0.021	750
<b>I2</b>	<b>0.865</b>	<b>0.039</b>	<b>375</b>
M7	0.865	0.039	750
M8	1.240	0.020	750
I3	1.610	0.060	375
M10	1.610	0.060	750
M11	2.250	0.050	750

\*Full width half maximum (FWHM)

### 2.3 Retrieval Strategy

The basic retrieval strategy of the NVPS system is to produce VIIRS gridded Vegetation Index (VI) products from VIIRS observations. First, VIIRS TOA and TOC reflectance data are gridded to 0.003 degree resolution and then composited in daily, weekly and 16-day (bi-weekly) periods. The reflectance data are aggregated to 0.036-degree and 0.009-degree resolutions and corresponding daily, weekly and bi-weekly NDVIs and EVIs are calculated from the aggregated reflectance data. The system produces the daily, weekly and bi-weekly VI products, respectively, at the global (0.036-degree resolution) and regional (0.009-degree resolution) gridded scales,

## 3. ALGORITHM DESCRIPTION

### 3.1 Processing Outline

The NVPS system generates daily, daily rolling weekly and daily rolling 16-day composite vegetation index products through the following steps:

Step 1: VIIRS swath TOA reflectance and TOC surface reflectance data in bands I1, I2, and M3 during a calendar day (0000 – 2400 UTC) are mapped to the native VI

geographic grid (0.003 degree Plate Carrée projection) to produce a gridded daily TOA reflectance and surface reflectance maps, respectively.

- Step 2: At the end of a 7-day (16-day) period, the daily surface reflectance maps of the 7 days (16 days) are composited to produce a weekly surface reflectance map using the maximum view-angle adjusted SAVI (MVA-SAVI) compositing algorithm, which selects, at each VI grid point (pixel), the observation with the maximum view-angle adjusted SAVI value in the 7-day (16-day) period. The 7-day (16-day) compositing is conducted daily using data in the previous 7 days (16 days) as input data, which is called daily rolling weekly (16-day) compositing. Cloud mask, aerosol, and sun/view angles of composited pixels are saved.
- Step 3: Daily, daily rolling weekly and 16-day composited TOA and TOC reflectances are aggregated to 0.009 degree and 0.036 degree resolutions.
- Step 4: TOA NDVI is calculated from the daily, daily rolling weekly and 16-day composited VIIRS TOA reflectance in bands I1, I2, respectively. TOC NDVI and TOC EVI are calculated from the daily, daily rolling weekly and 16-day composited VIIRS surface reflectance data in bands I1, I2 and M3, respectively. Quality Assurance (QA) information of the native VI grids is aggregated to 0.009 degree and 0.036 degree resolutions by certain rules. The TOA NDVI, TOC NDVI and TOC EVI and the aggregated reflectance and QA are written in output maps.

A high level algorithm processing flow is shown in Figure 1.

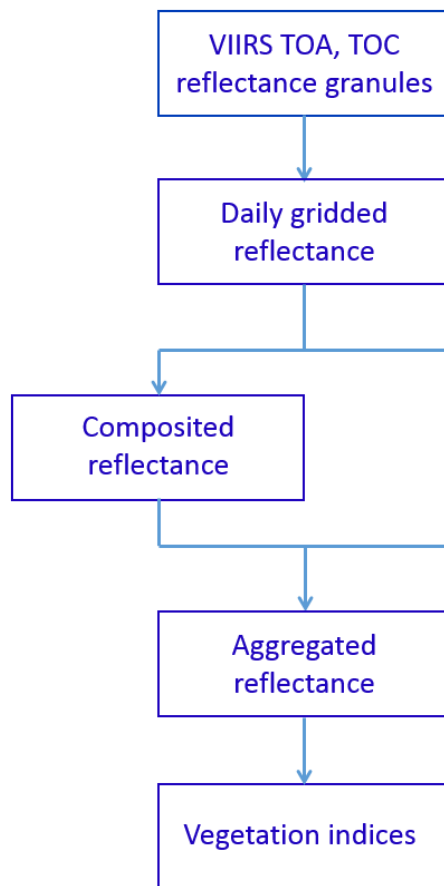


*Figure 1. Flow chart of VIIRS VI system.*

Notice of Figure 1:

“VIIRS TOA, TOC reflectance granules” include the TOA reflectance and the TOC reflectance in VIIRS bands I1, I2, and M3 for a VIIRS granule, obtained from the NOAA enterprise SR, SVI01 and SVI02 files.

“Daily gridded reflectance” is “VIIRS TOA and TOC reflectance” projected to the native GVF grid during a calendar day.

“Composited reflectance” is the daily rolling weekly and 16-day composite reflectance that is produced daily by Maximum Value Compositing of “daily gridded reflectance” in a 7-day and 16-day periods. This consists of the maximum view-angle adjusted SAVI value selected observation for each grid point (pixel).

“Aggregated reflectance” is the TOA and TOC reflectance aggregated to 0.009 degree and 0.036 degree grids.

“Vegetation indices” includes the TOA NDVI, TOC NDVI and TOC EVI.

### 3.2 Algorithm Input

The input data of the VIIRS VI system include the VIIRS TOC and TOA reflectance, geolocation, aerosol optical depth, cloud mask and land/water mask (table 3).

**Table 3. Input Data of the VIIRS VI System**

Name	File name	File format	Input type
VIIRS surface reflectance	SR	netCDF	Daily
VIIRS TOA reflectance I1 band	SVI01	HDF5	Daily
VIIRS TOA reflectance I2 band	SVI02	HDF5	Daily
VIIRS geolocation data	GITCO	HDF5	Daily
VIIRS aerosol optical depth	JRR-AOD	netCDF	Daily
Cloud mask	JRR-CloudMask	netCDF	Daily
MODIS land/water mask	MOD44W	HDF5	Static

#### 3.2.1 VIIRS surface reflectance data

The VIIRS surface reflectance is a granule file (IVISR) that contains TOC reflectance data in twelve VIIRS spectral bands listed in Table 2. The VI algorithm uses the red (I1), NIR (I2) and blue (M3) reflectance data to calculate The TOC NDVI and EVI. Cloud flag information is included in the IVISR files. Details of VIIRS surface reflectance RIP are available at [http://npp.gsfc.nasa.gov/sciencedocuments/ATBD\\_122011/474-00034\\_VIIRS-SurfReflect-ATBD\\_Rev-\\_22Apr2011.pdf](http://npp.gsfc.nasa.gov/sciencedocuments/ATBD_122011/474-00034_VIIRS-SurfReflect-ATBD_Rev-_22Apr2011.pdf)

#### 3.2.2 VIIRS TOA reflectance I1 data

The VIIRS TOA surface reflectance I1 is a granule file (SVI01) that contains radiance, reflectance and quality flag data in VIIRS I1 band. The VI algorithm uses the TOA red (I1) reflectance data to calculate TOC NDVI. Details of VIIRS sensor data record are available at

---

[https://www.star.nesdis.noaa.gov/smcd/spb/nsun/snpp/VIIRS/VIIRS\\_SDR\\_Users\\_guide.pdf](https://www.star.nesdis.noaa.gov/smcd/spb/nsun/snpp/VIIRS/VIIRS_SDR_Users_guide.pdf)

### **3.2.3 VIIRS TOA reflectance I2 data**

The VIIRS TOA surface reflectance I2 is a granule file (SVI02) that contains radiance, reflectance and quality flag data in VIIRS I2 band. The VI algorithm uses the TOA NIR (I2) reflectance data to calculate TOC NDVI. Details of VIIRS sensor data record are available at [https://www.star.nesdis.noaa.gov/smcd/spb/nsun/snpp/VIIRS/VIIRS\\_SDR\\_Users\\_guide.pdf](https://www.star.nesdis.noaa.gov/smcd/spb/nsun/snpp/VIIRS/VIIRS_SDR_Users_guide.pdf)

### **3.2.4 VIIRS geolocation data**

The VIIRS geolocation files (GITCO) include latitude and longitude and sun-view geometry information corresponding to the VIIRS Surface Reflectance. The VI algorithm uses the latitude and longitude information in gridding and the sun-view geometry information in compositing.

### **3.2.5 VIIRS Aerosol Optical Depth (AOD) data**

JPSS Risk Reduction Unique Aerosol Optical Depth (JRR-AOD) data provides the Aerosol optical depth at 550 nm. The VI algorithm reads the AOD Retrieval quality data and uses it in the quality assurance of the VIIRS VI products.

### **3.2.6 VIIRS cloud mask**

JPSS Risk Reduction Unique Cloud Mask (JRR-CloudMask) data provides the cloud mask of the VIIRS data. The VI algorithm reads the cloud mask data and uses it in the quality assurance of the VIIRS VI products.

### **3.2.7 MODIS land/water mask**

The Moderate Resolution Imaging Spectroradiometer (MODIS) 250-m land-water mask (MOD44W) was re-projected to the lat/lon projection and re-sampled to the VI grid resolution (see section 3.3.1). The land-water mask is used as a static input of the VI system to mask water pixels.

## ***3.3 Theoretical Description***

Vegetation indices are spectral transformations of two or more bands designed to enhance the contribution of vegetation properties and allow reliable spatial and temporal inter-

comparison of terrestrial photosynthetic activity and canopy structural variations (Huete et al., 2002). Although VIs are not intrinsic physical quantities, they are widely used as proxies in the assessment of many biophysical and biochemical variables, including canopy chlorophyll content (Blackburn, 1998; Gitelson et al., 2005), leaf area index (LAI) (e.g. Boegh et al., 2002; Chen & Cihlar, 1996), Green Vegetation Fraction (GVF) (e.g. Baret et al., 1995; Wittich and Hansing, 1995; Gutman & Ignatov, 1998; Jiang et al., 2006; Zeng et al., 2000), gross primary productivity (GPP) (Rahman et al., 2005; Sims et al., 2006), and fraction of photosynthetically active radiation absorbed by the vegetation (FAPAR) (e.g. Myneni et al., 1997; Di Bella et al., 2004; Baret et al., 2007).

Normalized difference vegetation index (NDVI) time series data products based on the Advanced Very High Resolution Radiometer (AVHRR) instruments, such as the GIMMS (Global Inventory Modeling and Mapping Studies) and Pathfinder AVHRR Land (PAL) datasets, are available from 1981, and have contributed significantly to global land processes studies, vegetation–climate interactions, and other advancements in Earth System Science (e.g. Defries & Belward, 2000; Suzuki et al., 2007; Townshend, 1994; Tucker et al., 1986). The main disadvantages of the NDVI include the sensitivity to the variation of soil background (Huete, 1988), the inherent nonlinearity of ratio-based indices (Huete et al., 2002; Jiang et al., 2006) and the influence of atmospheric path radiances (Kaufman 1997).

EVI was developed to optimize the vegetation signal with improved sensitivity in high biomass regions and improved vegetation monitoring through a de-coupling of the canopy background signal and a reduction in atmosphere influences (Huete et al., 2002). EVI has been used recently in a wide variety studies, including those on land cover/land use change (Wardlow et al., 2007), estimation of vegetation biophysical parameters (Chen et al., 2004; Houborg et al., 2007), phenology (Ahl et al., 2006; Xiao et al., 2006; Zhang et al., 2003), evapotranspiration (Nagler et al., 2005), biodiversity (Waring et al., 2006), and the estimation of gross primary production (GPP) (Rahman et al., 2005; Sims et al., 2008, 2006).

EVI not only gains its heritage from the soil-adjusted vegetation index (SAVI) (Huete, 1988) and the atmospherically resistant vegetation index (ARVI) (Kaufman and Tanré, 1992), but also improves the linearity with vegetation biophysical parameters, encompassing a broader range in leaf area index (LAI) retrievals (Houborg et al., 2007). It has been shown to be strongly linear related and highly synchronized with seasonal tower photosynthesis measurements in terms of phase and amplitude, with no apparent saturation observed over temperate evergreen needleleaf forests (Xiao et al., 2004), tropical broadleaf evergreen rainforests (Huete et al., 2006), and particularly temperate broadleaf deciduous forests (Rahman et al., 2005; Sims et al., 2006).

### 3.3.1 Gridding

The VI algorithm starts from VIIRS TOA and TOC reflectance granules and grid the data, using nearest-neighbor method, onto a global 0.003° (333-m) grid. This grid is based on the Plate Carrée map projection and consists of 120,000x60,000 grid points (pixels) in the global map, which spans from 90° (north edge) to -90° (south edge) in the latitudinal and from -180° (west) to 180° (east) in longitude directions.

### 3.3.2 Compositing

The VI algorithm input includes the VIIRS TOA and TOC reflectance and geo-location data for each granule. Daily I1, I2, and M3 surface reflectance data in a 7-day or 16-day period are composited at 1-day interval (daily rolling weekly or 16-day). A daily rolling weekly (16-day) compositing period can start at any day of a year and covers 7 days (16 days). The next compositing period shifts one day after the last 7-day (16-day) period. At the end of a year, a compositing period cover some days in the next year if there are not enough days left in the year. The end result of composting over a 7-day (16-day) period is a single file containing, for each 0.003 degree grid point, TOA and TOC red (I1), NIR (I2), TOC blue (M3) reflectance, sensor and solar zenith angles, relative azimuth angle, and quality flags in a HDF5 file.

The compositing procedure developed for the NOAA VIIRS GVF system is adopted in the VIIRS VI system, which is different from the traditional maximum value compositing (MVC) procedure used in the GVPS system. It is well documented that MVC based on NDVI favors observations in the forward scatter direction, creating a bias and resulting in low red and NIR reflectances because of shadowing effect (Cabral et al., 2003; Carreiras et al., 2003; van Leeuwen et al., 1999; Stoms et al., 1997; Cihlar et al., 1994; Huete et al., 1992; Gutman, 1991). To reduce the bias, the soil-adjusted vegetation index (SAVI), with varying soil adjustment factor (L) values, is proposed and tested for MVC using the MYD09GA data (i.e. VIIRS surface reflectance proxy data). It was found that L had great impact on the selection of the composited data. With the increase of the L value from 0 to 0.5, the bias shifted from the forward scatter direction to the backscatter direction (Fig. 2). Mean EVI values composited based on SAVI are greater than those composited based on NDVI (L=0) (Fig. 3). The SAVI with L=0.05 was found to be the optimal vegetation index used in compositing to minimize the bias between the two directions (Fig. 2).

$$SAVI = (1 + L) \frac{\rho_{NIR} - \rho_{red}}{\rho_{NIR} + \rho_{red} + L} \quad (3.1)$$

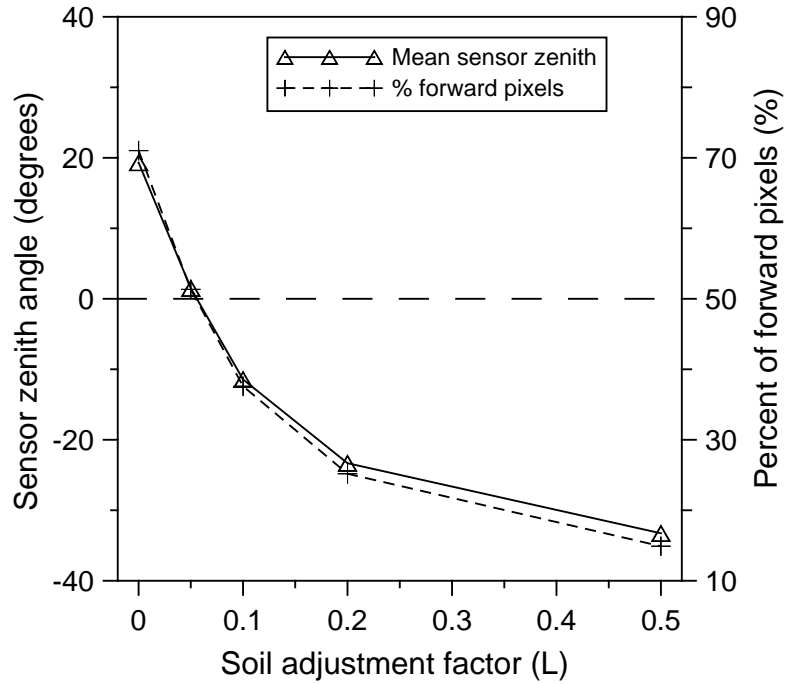


Figure 2. Yearly mean sensor zenith angles and yearly mean percentage of forward scatter direction pixels of the maximum SAVI composited images over the tile H10V05 in 2007 as functions of the soil adjustment factor (L) values.

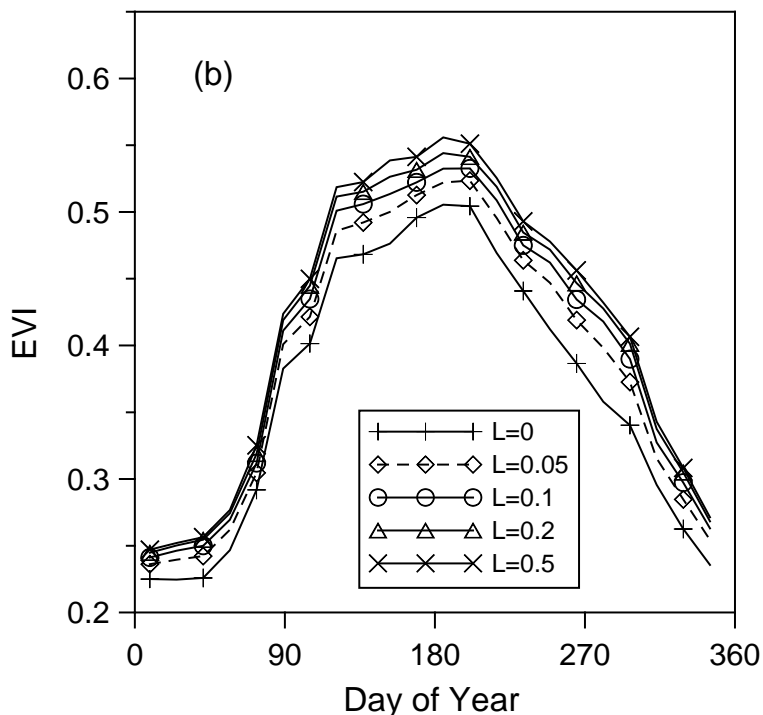
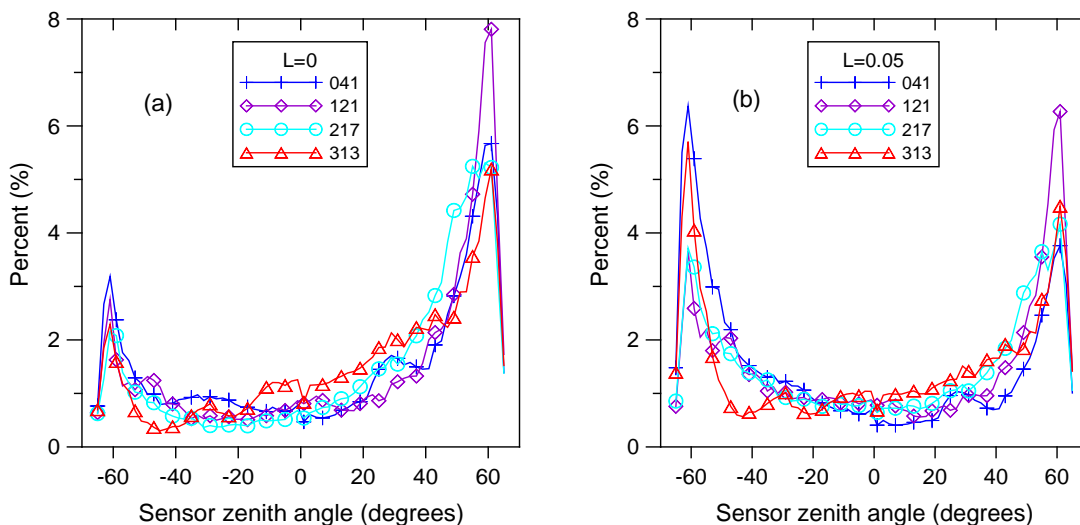


Figure 3. Mean EVI composited by the maximum SAVI method using the five soil adjustment factor ( $L$ ) values over the tile H10V05 in 2007.

Although the bias in the view angle directions can be successfully minimized by the MVC based on SAVI ( $L=0.05$ ), most of pixels composited by MVC are from high sensor zenith angles, regardless of whatever  $L$  values are used in compositing (Fig. 4). In some cases, the maximum NDVI is selected at the expense of optimal view geometry since sensor zenith angles selected by MVC are often further off-nadir than necessary to ensure cloud-free viewing (Stoms et al, 1997). This is an inherent limitation of MVC since more vegetation canopies and fewer gaps among canopies can be observed from high view zenith angles than from the nadir view.



*Figure 4. Histograms of the sensor zenith angles composited by the traditional MVC based on NDVI ( $L=0$ ) (a) and by the MVC based on SAVI ( $L=0.05$ ) in different seasons (compositing periods beginning at DOYs 041, 121, 217 and 313) in 2007 over the tile H10V05.*

Thus, sensor zenith angles should be taken into account in compositing such that observations close to the nadir view are given a priority under clear sky conditions and observations at off-nadir view should be selected only if nadir view observations are cloudy. So, in compositing, SAVI should be adjusted according to the sensor zenith angle for each observation. The view-angle adjusted SAVI (VA-SAVI) is

$$VA-SAVI = SAVI - C \times SZ^2 \quad (3.2)$$

where  $SZ$  is the sensor zenith angle in degrees and  $C$  is a coefficient that accounts for the view angle variation of SAVI. The view angle variation of SAVI and other VIs is associated with the bidirectional reflectance distribution function (BRDF) of surface. The BRDF effects are prominent over heterogeneous surface with intermediate vegetation density and insignificant over homogeneous surface, such as bare soil or fully vegetated area. So  $C$  is a function of vegetation density, which can be estimated by the maximum SAVI ( $SAVI_{max}$ ) in a compositing period for a pixel.

$$C = C_1 - C_2(SAVI_{max} - 0.5)^2 \quad (3.3)$$

Where  $C_1=0.00008$  and  $C_2=0.0002$ . The  $C$  value is highest ( $0.00008$ ) when  $SAVI_{max}=0.5$  and becomes  $0.3$  when  $SAVI_{max}=1$  or  $0$  (Fig. 5). It should be noted that the  $C$  values are very small because the unit of sensor zenith angles in Eq. 3.2 is the degree.

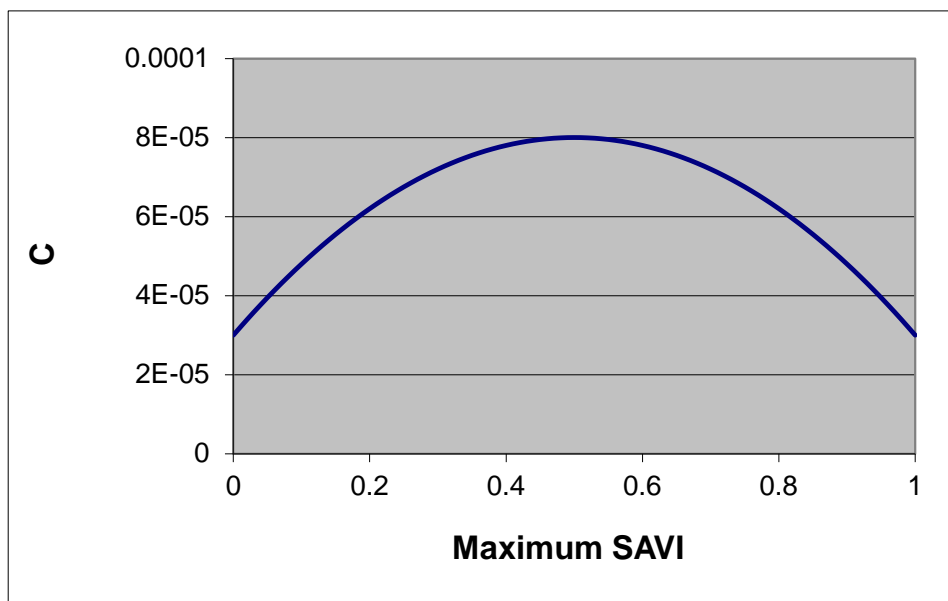


Figure 5.  $C$  is designed as a function of the maximum SAVI.

Instead of selecting the maximum NDVI, the VI compositing algorithm selects the maximum view-angle adjusted SAVI (MVA-SAVI) in a compositing period for each pixel. Fig. 6 shows an example of the MVA-SAVI compositing, compared with the traditional MVC. In the compositing period, only one day of observation is cloudy and the other six days are cloud-free. MVC selects the maximum NDVI observation at sensor zenith angle  $52^\circ$  in the forward scatter direction. Whereas the MVA-SAVI compositing method selects the observation closest to the nadir view since VA-SAVI values are reduced according to the sensor zenith angles. The higher sensor zenith angles, the smaller VA-SAVI values.

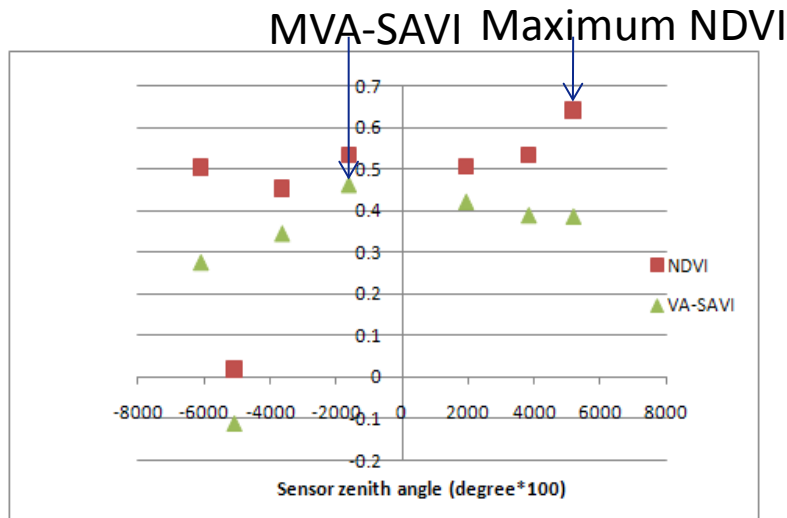


Figure 6. Comparison of the maximum value compositing and the maximum view angle adjusted SAVI compositing.

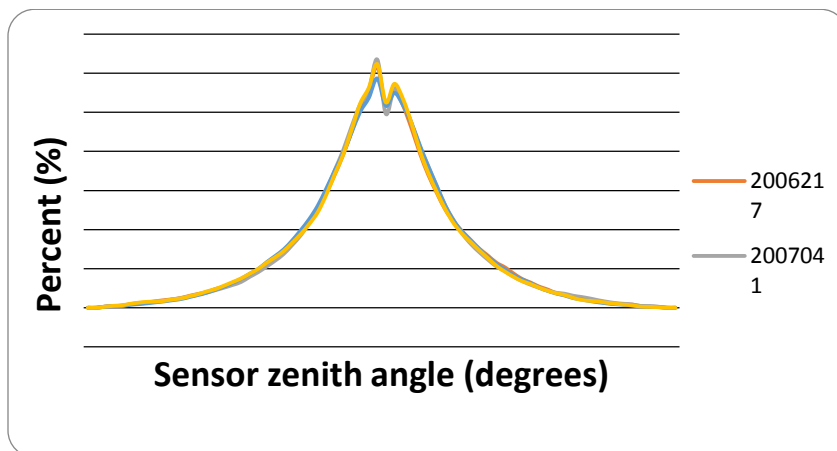


Figure 7. Histograms of sensor zenith angles composited by the MVA-SAVI method at different seasons.

---

The peaks of the histograms of sensor zenith angles composited by the MVA-SAVI method are close to the nadir at different seasons, indicating that observations close to the nadir view are likely selected than the off-nadir observations (Fig. 7).

### 3.3.3 Reflectance aggregation

The daily gridded reflectance, daily rolling weekly and 16-day composite TOA and TOC reflectance data at the  $0.003^\circ$  grid are aggregated  $3 \times 3$  to a  $0.009^\circ$  grid ( $\sim 1$  km) based on the spatial average method. The daily gridded reflectance, daily rolling weekly and 16-day composite TOA and TOC reflectance data at the  $0.003^\circ$  grid are also aggregated  $12 \times 12$  to a  $0.036^\circ$  grid ( $\sim 4$  km) based on the spatial average method.

### 3.3.4 VI calculation

TOA NDVI is calculated using the aggregated TOA reflectance and TOC NDVI is calculated using the aggregated TOC reflectance at 1-km and 4-km resolutions respectively.

$$NDVI = \frac{\rho_{NIR} - \rho_{red}}{\rho_{NIR} + \rho_{red}} \quad (3.4)$$

TOC EVI is calculated using the aggregated TOC reflectance at 1-km and 4-km resolutions respectively.

$$EVI = G \frac{\rho_{NIR} - \rho_{red}}{\rho_{NIR} + C_1 \rho_{red} - C_2 \rho_{blue} + L} \quad (3.5)$$

where  $\rho_{NIR}$ ,  $\rho_{red}$ ,  $\rho_{blue}$  are the TOC NIR, red and blue reflectances respectively,  $L$  is the canopy background adjustment that addresses nonlinear, differential NIR and red radiant transfer through a canopy, and  $C_1$ ,  $C_2$  are the coefficients of the aerosol resistance term, which uses the blue band to correct for aerosol influences in the red band. The coefficients adopted in the EVI algorithm are,  $L=1$ ,  $C_1=6$ ,  $C_2 = 7.5$ , and  $G$  (gain factor) = 2.5 (Huete, et al., 2002; Liu and Huete, 1995).

---

Due to the use of blue band, the denominator of the EVI equation could be equal to, or very close to, 0 and EVI values are abnormal under certain circumstance. For example, when  $\rho_{red}=0.2380$ ,  $\rho_{NIR}=0.2255$  and  $\rho_{blue}=0.3538$ , the EVI value becomes infinite. A two-band EVI (EVI2) without a blue was developed by Jiang et al. (2008), which is robust under any circumstance and has the best similarity with the 3-band EVI.

$$EVI2 = 2.5 \frac{\rho_{NIR} - \rho_{red}}{\rho_{NIR} + 2.4\rho_{red} + 1} \quad (3.6)$$

If the red/blue ratio is less than 1.25, or the blue reflectance is larger than 0.3, or EVI is larger than 0.7 or smaller than 0, then the EVI values are replaced by EVI2 values calculated using Eq. (3.6).

### 3.3.5 VI QA assignment

The daily gridded TOA and TOC reflectances and the derived VI products are subject to impact of environmental factors including cloud, aerosol and Sun glint. Hence the quality assurances of derived VI products on the aggregated pixels are based on the quality assurances stored as QF1 through QF7 in VIIRS Surface Reflectance data files and Aerosol Optical Thickness data files at granule level, and spatial aggregation scheme. The following section 3.3.5.1 introduces QFs of VIIRS data at granule level. The section 3.3.5.2 describes spatial aggregation scheme for NDE (Enterprise) VIIRS VI products. The section 3.3.5.3 summarizes the aggregation QFs in table.

#### 3.3.5.1. Granule level QFs of NDE (Enterprise) VIIRS data

There are seven granule level quality flags in the VIIRS Surface Reflectance file, listed as QF1 through QF7. These fields are bit-mapped quality fields for the inputs and outputs of the algorithm. These are listed in Table 4 through 10. Tables are ordered from the most significant bit (7) to the least significant bit (0).

**Table 4. QF1 Surface Reflectance**

<b>Bit #</b>	<b>Meaning</b>
6-7	Sun Glint 00: no sun glint detected 11: sun glint detected
5	Low Sun Mask 0: high 1: low
4	Day/Night Flag 0: day 1: night
<b>2-3</b>	Cloud Detection and Confidence 00: confidently clear 01: probably clear 10: probably cloudy 11: confidently cloudy
<b>0-1</b>	Cloud Mask Quality

**Table 5. QF2 Surface Reflectance**

Bit #	Meaning
7	Thin Cirrus Detected – Emissive Test 0: no cloud 1: cloud
6	Thin Cirrus Detected – Reflective Test 0: no cloud 1: cloud
5	Snow/Ice Flag 0: no snow/ice 1: snow or ice
4	Heavy Aerosol Mask 0: no heavy aerosol 1: heavy aerosol
3	Cloud Shadow Mask 0: no cloud shadow 1: shadow
0-2	Land/Water Mask 001: deep ocean 010: shallow water 011: land 100: snow 101: arctic 110: Antarctic and Greenland 111: desert

**Table 6. QF3 Surface Reflectance**

<b>Bit #</b>	<b>Meaning</b>
7	Bad M10 SDR data 0: no 1: yes
6	Bad M8 SDR data 0: no 1: yes
5	Bad M7 SDR data 0: no 1: yes
4	Bad M5 SDR data 0: no 1: yes
3	Bad M4 SDR data 0: no 1: yes
2	Bad M3 SDR data 0: no 1: yes
1	Bad M2 SDR data 0: no 1: yes
0	Bad M1SDR data 0: no 1: yes

**Table 7. QF4 Surface Reflectance**

---

Bit #	Meaning
7	Missing Perceptible Water data 0: no 1: yes
6	Invalid Land AM input data 0: valid 1: invalid or over ocean
5	Missing AOT input data 0: no 1: yes
4	Overall Quality of AOT 0: good 1: bad
3	Bad I3 SDR data 0: no 1: yes
2	Bad I2 SDR data 0: no 1: yes
1	Bad I1 SDR data 0: no 1: yes
0	Bad M11 SDR data 0: no 1: yes

**Table 8. QF5 Surface Reflectance**

---

---

Bit #	Meaning
7	Overall Quality of M7 Surface Reflectance Data 0: good 1: bad
6	Overall Quality of M5 Surface Reflectance Data 0: good 1: bad
5	Overall Quality of M4 Surface Reflectance Data 0: no 1: yes
4	Overall Quality of M3 Surface Reflectance Data 0: no 1: yes
3	Overall Quality of M2 Surface Reflectance Data 0: good 1: bad
2	Overall Quality of M1 Surface Reflectance Data 0: no 1: yes
1	Missing Surface Pressure Input Data 0: no 1: yes
0	Missing Total Column Ozone Input Data 0: no 1: yes

**Table 9. QF6 Surface Reflectance**

---

---

Bit #	Meaning
7	unread
6	unread
5	Overall Quality of I3 Surface Reflectance Data 0: good 1: bad
4	Overall Quality of I2 Surface Reflectance Data 0: good 1: bad
3	Overall Quality of I1 Surface Reflectance Data 0: good 1: bad
2	Overall Quality of M11 Surface Reflectance Data 0: good 1: bad
1	Overall Quality of M10 Surface Reflectance Data 0: good 1: bad
0	Overall Quality of M8 Surface Reflectance Data 0: good 1: bad

**Table 10. QF7 Surface Reflectance**

Bit #	Meaning
7	unread
6	unread
5	unread
4	Thin Cirrus Flag 0: no 1: yes
2-3	Aerosol Quality 00: climatology 01: low 10: average 11: high
1	Adjacent to Cloud (disabled) 0: no 1: yes
0	Snow Present 0: no 1: yes

### 3.3.5.2. Spatial aggregation scheme for quality assurance of VIIRS VI products

In consideration of Quality Flags (QFs), the following spatial averaging scheme is proposed:

#### Step 1: Cloud flag

If the number of pixels with “confidently clear” is greater than or close to 80% of pixels (i.e.,  $n \geq 7$  for aggregating into 0.009°-grid, and  $n \geq 115$  for aggregating into 0.036°-grid), then average only those “confidently clear” pixels and set Cloud Flag on the aggregated pixel as “confidently clear”.

If the number of pixels with “confidently clear or probably clear” is greater than or close to 80% of pixels (i.e.,  $n \geq 7$  for aggregating into 0.009°-grid, and  $n \geq 115$  for aggregating into 0.036°-grid), then average only those “confidently clear or probably” pixels and set Cloud Flag on the aggregated pixel as “probably clear”.

If the number of pixels with “confidently clear or probably clear or probably cloudy” is greater than or close to 80% of pixels (i.e.,  $n \geq 7$  for aggregating into 0.009°-grid, and  $n \geq 115$  for aggregating into 0.036°-grid), then average only those “confidently clear or probably clear or probably cloudy” pixels and set Cloud Flag on the aggregated pixel as “probably cloudy”.

Otherwise, average all pixels and set Cloud Flag on the aggregated pixel as “confidently cloudy”.

### Step 2: Sun/View angle

There are (i) sun zenith angle, (ii) view zenith angle, (iii) relative azimuth angle. For each of these angles, angle values of pixels used for averaging in step 1 will be averaged to represent the angle value for the aggregated pixel.

### Step 3: Land/Water mask (LWM)

LWM QF values of aggregated pixels will be determined by the following rules:

- If any of pixels averaged in step 1 is “snow”, set LWM value to “snow”.
- If all pixels averaged in step 1 are “deep ocean”, set LWM value to “Deep Ocean”.
- If majority pixels averaged in step 1 are “Deep Ocean” and at least one shallow water and no snow”, set LWM value to “shallow water”.
- If majority pixels averaged in step 1 are “land and no snow”, set LWM value to “land”.
- If majority pixels averaged in step 1 are “arctic and no snow”, set LWM value to “arctic”.
- If majority pixels averaged in step 1 are “Antarctic and Greenland and no snow”, set LWM value to “Antarctic and Greenland”.
- If majority pixels averaged in step 1 are “desert and no snow”, set LWM value to “desert”.

Step 4: Values for other QFs for aggregated pixels will be determined by either “majority” or “worst case scenario”:

AOT >1.0: use the majority value among pixels used for averaging in step 1.

# NOAA NESDIS STAR

ALGORITHM THEORETICAL BASIS DOCUMENT

Version: 1.0

Date: Feb. 2, 2018

TITLE: VIIRS VI Algorithm Theoretical Basis Document

Page 37 of 64

Aerosol Quantity: use the majority value among pixels used for averaging in step 1.

Snow/ice: set to “1” if any pixel used for averaging in step 1 has “snow/ice =1”.

Adjacent to Cloud: set to “1” if any one pixels used for averaging in step 1 has “adjacent to Cloud = 1”.

Thin Cirrus: set to “1” if any pixel used for averaging in step 1 has “Thin Cirrus = 1”.

Cloud Shadow: set to “1” if any one pixels used for averaging in Step 1 has “Cloud Shadow = 1”.

Sun Glint: Sun Glint QF should be assigned only 1-bit for aggregated pixels. Over land, only the “geometry-based” detection is used. Set to “1” if any pixel used for averaging in Step 1 has “Sun Glint = 01 (Geometry-based)”.

### 3.3.5.3. QFs of VIIRS VI products

There are four QFs in the NVPS VI output files, listed as QF1 through QF4. These fields are bit-mapped quality fields for the inputs and outputs of the algorithm. They are listed in Table 11.

**Table 11. Bit Layout of the Four QFs in the NVPS VI Product**

Byte	VIIRS VI Flag	Result	Bits
0	Overall TOA NDVI Quality	1 = High 0 = Low NOTE: TOA NDVI quality is set to high (1) if ALL of these conditions are met: 1) I1 TOA reflectance flag = avail ; 2) I2 TOA reflectance flag = avail 3) Cloud Confidence flag = confidently clear 4) Thin Cirrus flag = no thin cirrus; 5) Solar Zenith Angle < 65 deg 6) Sun glint (Geometry based) = none; 7) No adjacency clouds 8) No cloud shadows; 9) No snow/ice 10) Aerosol quantity = “low” or “medium” or “climatology” 11) Cloud mask quality = “high” or “medium”	1
	Overall TOC EVI Quality	1 = High 0 = Low NOTE: EVI quality is set to high (1) if ALL of these conditions are met:	1

# NOAA NESDIS STAR

## ALGORITHM THEORETICAL BASIS DOCUMENT

Version: 1.0

Date: Feb. 2, 2018

TITLE: VIIRS VI Algorithm Theoretical Basis Document

Page 38 of 64

		1) I1 Surface reflectance flag = avail ; 2) I2 Surface reflectance flag = avail 3) M3 Surface reflectance flag = avail; 4) Cloud Confidence flag = confidently clear; 5) Thin Cirrus flag = no thin cirrus; 6) Solar Zenith Angle < 65 deg 7) Sun glint (Geometry based) = none; 8) EVI range flag = in range 9) No adjacency clouds; 10) No cloud shadows 11) No snow/ice; 12) Aerosol quantity = "low" or "medium" or "climatology" 13) Cloud mask quality = "high" or "medium"	
	Overall TOC NDVI Quality	1 = High 0 = Low NOTE: TOC NDVI quality is set to high (1) if ALL of these conditions are met: 1) I1 Surface reflectance flag = avail ; 2) I2 Surface reflectance flag = avail 3) Cloud Confidence flag = confidently clear; 4) Thin Cirrus flag = no thin cirrus; 5) Solar Zenith Angle < 65 deg 6) Sun glint (Geometry based) = none 7) No adjacency clouds 8) No cloud shadows 9) No snow/ice 10) Aerosol quantity = "low" or "medium" or "climatology" 11) Cloud mask quality = "high" or "medium"	1
	I1 TOA Reflectance	1 = Not Available 0 = Available	1
	I2 TOA Reflectance	1 = Not Available 0 = Available	1
	I1 Surface Reflectance	1 = Not Available 0 = Available	1
	I2 Surface Reflectance	1 = Not Available 0 = Available	1
	M3 Surface Reflectance	1 = Not Available 0 = Available	1
1	EVI Range	1 = Out of Range 0 = In Range	1
	*Land/Water	001= deep ocean (1) 010= shallow water (2) 011= land (3) 100= snow (4) 101= arctic (5) 110= Antarctic + Greenland (6) 111= desert (7)	3

# NOAA NESDIS STAR

## ALGORITHM THEORETICAL BASIS DOCUMENT

Version: 1.0

Date: Feb. 2, 2018

TITLE: VIIRS VI Algorithm Theoretical Basis Document

Page 39 of 64

	*Cloud Confidence	11 = Confidently Cloudy 10 = Probably Cloudy 01 = Probably Clear 00 = Confidently Clear	2
	*Sun Glint	11 = Geometry & Wind 10 = Wind Speed Based 01 = Geometry Based 00 = None	2
2	*Thin Cirrus (reflective)	1 = Cloud 0 = No Cloud	1
	Stratification – Solar Zenith Angle	1 = 65 Degrees <= SZA <= 85 Degrees 0 = SZA < 65 Degrees or SZA > 85 Degrees	1
	*Excl – AOT > 1.0	1 = AOT > 1.0 0 = AOT <= 1.0	1
	Excl – Solar Zenith Angle > 85 Deg	1 = SZA > 85 degrees 0 = SZA <= 85 degrees	1
	*Snow/Ice	0 = False (no) 1 = True (yes)	1
	*Adjacent to Clouds	0 = False (no) 1 = True (yes)	1
	*Aerosol Quantity	00 = Climatology 01 = Low 10 = Average 11 = High	2
3	*Cloud Shadows	0 = False (no) 1 = True (yes)	1
	**Aerosol Optical Thickness Quality	00 = High Quality 01 = Degraded Quality 10 = Excluded Quality 11 = Not Produced	2
	*Cloud Mask Quality	00 = Poor 01 = Low 10 = Medium 11 = High	2
	Spare Bits	Initialized to 0	3

### 3.4 Algorithm Output

The outputs of VIIRS VI system consists of three VI products, including TOA NDVI, TOC NDVI and TOC EVI, at three composite periods (i.e. daily, daily rolling weekly and daily rolling

# NOAA NESDIS STAR

## ALGORITHM THEORETICAL BASIS DOCUMENT

Version: 1.0

Date: Feb. 2, 2018

TITLE: VIIRS VI Algorithm Theoretical Basis Document

Page 40 of 64

16-day), at two spatial resolutions (i.e. 4-km in global map and 1-km in regional map). For each composite period, the VIIRS VI system outputs include:

- (1) 4-km global TOA NDVI, TOC NDVI, TOC EVI, TOA I1 (red) reflectance, TOA I2 (NIR) reflectance, TOC I1 reflectance, TOC I2 reflectance, TOC M3 (blue) reflectance, QF1 through QF4, solar zenith angle, view zenith angle and relative azimuth angle on a global geographic projection grid stored in a NetCDF file.
- (2) 1-km regional TOA NDVI, TOC NDVI, TOC EVI, TOA I1 (red) reflectance, TOA I2 (NIR) reflectance, TOC I1 reflectance, TOC I2 reflectance, TOC M3 (blue) reflectance, QF1 through QF4, Solar zenith angle, view zenith angle and relative azimuth angle on a geographic projection grid stored in a NetCDF file.
- (3) Color-coded browse images of the global and regional TOA NDVI, TOC NDVI, TOC EVI maps, stored in six Geo-TIFF files.
- (4) Metadata: VI statistical data (maximum, minimum, mean and standard deviation over selected areas), which are useful for OSPO to monitor the VI product data quality and processing status, are saved in text files.

Table 12 lists all VIIRS VI output files and their characteristics.

**Table 12. VIIRS VI Output Files**

File	Description	Format	Size/file
VI-[DLY,WKL,BWKL]-REG _vxry_npp_s[YYYYMMDD1]_e[YYYYMMDD1,7 or 16]_c[YYYYMMDDhhmmsss].nc	This is the daily, weekly or biweekly regional VI product	netCDF4	Typical file size 1.6 GB.
VI-[DLY,WKL,BWKL]-GLB _vxry_npp_s[YYYYMMDD1]_e[YYYYMMDD1,7 OR 16]_c[YYYYMMDDhhmmsss].nc	This is the daily, weekly or biweekly global VI product	netCDF4	Typical file size 245 MB.
VI-TOA-NDVI-[DLY,WKL,BWKL]-REG _vxry_npp_s[YYYYMMDD1]_e[YYYYMMDD1,7 OR 16]_c[YYYYMMDDhhmmsss].tif	Browse image of the TOA NDVI regional VI product	Geotiff	Typical file size 45 MB
VI-TOA-NDVI-[DLY,WKL,BWKL]-GLB _vxry_npp_s[YYYYMMDD1]_e[YYYYMMDD1,7 OR 16]_c[YYYYMMDDhhmmsss].tif	Browse image of the TOA NDVI daily, weekly or biweekly global VI product	Geotiff	Typical file size 7 MB
VI-TOC-NDVI-[DLY,WKL,BWKL]-REG _vxry_npp_s[YYYYMMDD1]_e[YYYYMMDD1,7 OR 16]_c[YYYYMMDDhhmmsss].tif	Browse image of the TOC NDVI daily, weekly or biweekly regional VI product	Geotiff	Typical file size 45 MB
VI-TOC-NDVI-[DLY,WKL,BWKL]-GLB _vxry_npp_s[YYYYMMDD1]_e[YYYYMMDD1,7 OR 16]_c[YYYYMMDDhhmmsss].tif	Browse image of the TOC NDVI daily, weekly or biweekly global VI product	Geotiff	Typical file size 7 MB
VI-TOC-EVI-[DLY,WKL,BWKL]-REG	Browse image of the TOC	Geotiff	Typical file

# NOAA NESDIS STAR

## ALGORITHM THEORETICAL BASIS DOCUMENT

Version: 1.0

Date: Feb. 2, 2018

TITLE: VIIRS VI Algorithm Theoretical Basis Document

Page 41 of 64

_vxry_npp_s[YYYYMMDD1]_e[YYYYMMDD1,7 OR 16]_c[YYYYMMDDhhmmsss].tif	EVI daily, weekly or biweekly regional VI product		size 45 MB
VI-TOC-EVI-[DLY,WKL,BWKL]-GLB _vxry_npp_s[YYYYMMDD1]_e[YYYYMMDD1,7 OR 16]_c[YYYYMMDDhhmmsss].tif	Browse image of the TOC EVI daily, weekly or biweekly global VI product	Geotiff	Typical file size 7 MB
VI-[DLY,WKL,BWKL]-REG _vxry_npp_s[YYYYMMDD1]_e[YYYYMMDD1,7 OR 16]_c[YYYYMMDDhhmmsss].stat.txt	Statistics file of the daily, weekly or biweekly regional VI product for monitoring purposes	text	Typical file size 2 KB
VI-[DLY,WKL,BWKL]-GLB _vxry_npp_s[YYYYMMDD1]_e[YYYYMMDD1,7 OR 16]_c[YYYYMMDDhhmmsss].stat.txt	Statistics file of the daily, weekly or biweekly global VI product for monitoring purposes	text	Typical file size 2 KB

Table 13 lists VIIRS VI output file standard name description.

**Table 13. VIIRS VI Output Files Standard Name Description**

Sequence	Description
VI	Vegetation Indices (NDVI, EVI)
NDVI	Normal Difference Vegetation Index
EVI	Enhanced Vegetation Index
DLY	Daily (1-day temporal scale)
WKL	Weekly (7-day temporal resolution)
BWKL	Biweekly (16-day temporal resolution, in term of conventions )
GLB	Global (spatial resolution: 4-km)
REG	Regional (spatial resolution:1-km)
TOA	Top of Atmosphere
TOC	Top of Canopy
vxry	Version (e.g., v1r0)
npp	Indicates the observations from S-NPP
s	start (data observation time)
e	end (data observation time)
c	current (data processing time)
YYYYMMDD	4-digit year, 2-digit month, and 2-digit day
hhmmsss	2-digit hour, 2-digit minute, 2-digit second, and 1-digit fractional second
.nc	netCDF4 file
.tif	GeoTiff image file

stat.txt	Text file stored statistics analysis results
----------	--

The data structure of the VIIRS VI product includes the following data fields:

- 1) Three VI Products: NDVI\_TOA, EVI\_TOC and NDVI\_TOC;
- 2) Five reflectance bands: I1\_TOA, I2\_TOA, I1\_TOC, I2\_TOC, and M3\_TOC
- 3) Geometry Information: RAA: Relative Azimuth Angle, SZA: Solar Zenith Angle, and VZA: Viewing Zenith Angle;
- 4) Four Quality Flags (QFs).
- 5) Geospatial Coordinates: latitude, longitude

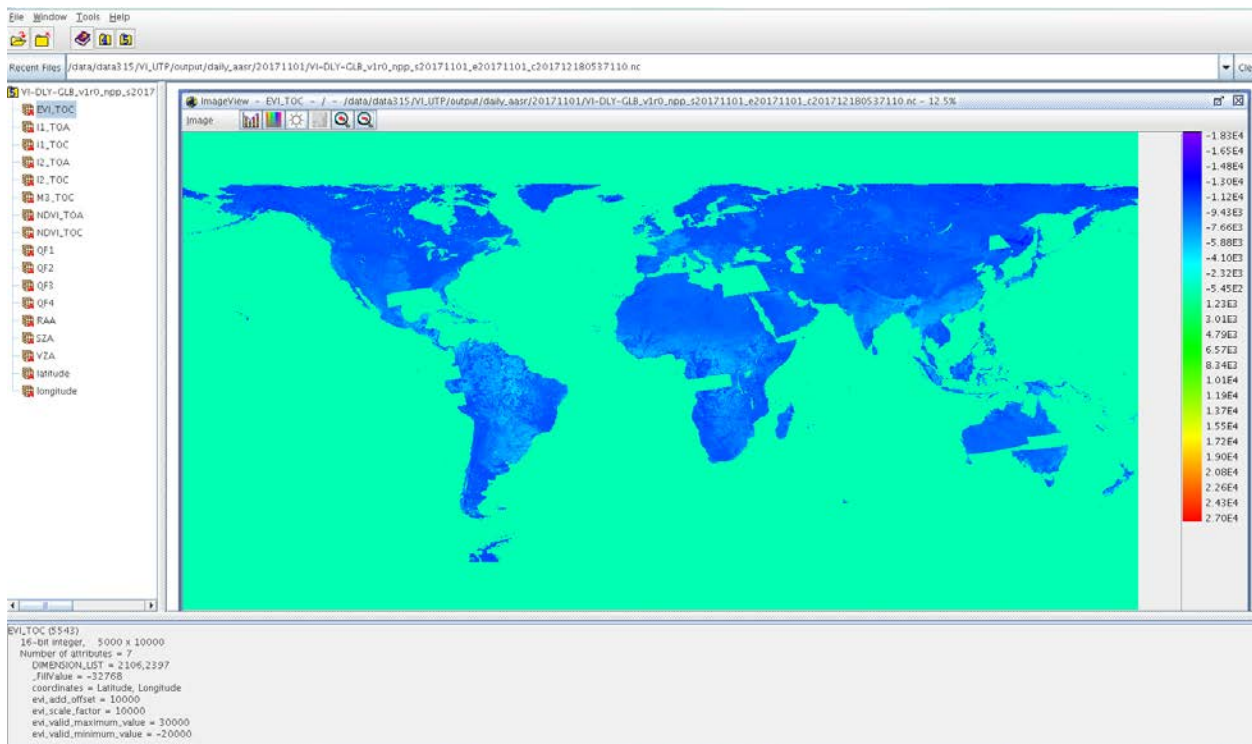


**Figure 8. Data fields of the VIIRS daily global VI product.**

Fig. 8 shows the data layers of the VIIRS VI output files. The description of these data fields are listed in Table 14. The details of the bit layout of the four quality flags are listed in Table 11 in Section 3.3.5.

# NOAA NESDIS STAR

## ALGORITHM THEORETICAL BASIS DOCUMENT

Version: 1.0

Date: Feb. 2, 2018

TITLE: VIIRS VI Algorithm Theoretical Basis Document

Page 43 of 64

**Table 14. Data Fields of the NVPS VI Product**

<b>Date Name</b>	<b>Data Description</b>	<b>Data Type</b>	<b>Dimension</b>	<b>Fill value</b>	<b>Scale</b>	<b>Offset</b>	<b>Data Range</b>
NDVI_TOA	Top of Atmosphere Normalized Difference Vegetation Index	16-bit Integer	5000x10000 (Global) 10384x28889 (Regional)	-32768	10000	0	[-1, 1]
NDVI_TOC	Top of Canopy Normalized Difference Vegetation Index	16-bit Integer	5000x10000 (Global) 10384x28889 (Regional)	-32768	10000	0	[-1, 1]
EVI_TOC	Top of Canopy Enhanced Vegetation Index	16-bit Integer	5000x10000 (Global) 10384x28889 (Regional)	-32768	10000	0	[-1, 1]
I1_TOA	Top of Atmosphere Reflectance band	16-bit Integer	5000x10000 (Global) 10384x28889 (Regional)	-32768	10000	0	[0, 1]
I2_TOA	Top of Atmosphere Reflectance band	16-bit Integer	5000x10000 (Global) 10384x28889 (Regional)	-32768	10000	0	[0, 1]
I1_TOC	Top of Canopy Reflectance band	16-bit Integer	5000x10000 (Global) 10384x28889 (Regional)	-32768	10000	0	[0, 1]
I2_TOC	Top of Canopy Reflectance band	16-bit Integer	5000x10000 (Global) 10384x28889 (Regional)	-32768	10000	0	[0, 1]
M3_TOC	Top of Canopy Reflectance band	16-bit Integer	5000x10000 (Global) 10384x28889 (Regional)	-32768	10000	0	[0, 1]
SZA	Solar Zenith Angle	16-bit Integer	5000x10000 (Global) 10384x28889 (Regional)	-32768	100	0	[0,90]

# NOAA NESDIS STAR

## ALGORITHM THEORETICAL BASIS DOCUMENT

Version: 1.0

Date: Feb. 2, 2018

TITLE: VIIRS VI Algorithm Theoretical Basis Document

Page 44 of 64

VZA	Viewing Zenith Angle	16-bit Integer	5000x10000 (Global) 10384x28889 (Regional)	-32768	100	0	[0,90]
RAA	Relative Azimuth Angle	16-bit Integer	5000x10000 (Global) 10384x28889 (Regional)	-32768	100	0	[-180,180]
QF1	Quality Flag Byte 0 (See Table 3-5)	8-bit unsigned character	5000x10000 (Global) 10384x28889 (Regional)	255	1	0	[0, 255]
QF2	Quality Flag Byte 1 (See Table 3-5)	8-bit unsigned character	5000x10000 (Global) 10384x28889 (Regional)	2	1	0	[0, 255]
QF3	Quality Flag Byte 2 (See Table 3-5)	8-bit unsigned character	5000x10000 (Global) 10384x28889 (Regional)	0	1	0	[0, 255]
QF4	Quality Flag Byte 3 (See Table 3-5)	8-bit unsigned character	5000x10000 (Global) 10384x28889 (Regional)	0	1	0	[0, 255]
Latitude	Geospatial coordinate	32-bit float	5000x1 (Global) 10384x1 (Regional)	-999.0	1	0	[-90,90] [-7.5,90]
Longitude	Geospatial coordinate	32-bit float	10000x1 (Global) 28889x1 (Regional)	-999.0	1	0	[-180,180] 130E->30E

The overall Meta information of the NVPS VI Product is shown in Table 15.

**Table 15. Meta Information of the NVPS VI Product**

Number of attributes = 29 Conventions = CF-1.5 Metadata_Conventions = CF-1.5, Unidata Dataset Discovery v1.0 cdm_data_type = grid creator_email = yunyue.yu@noaa.gov/marco.vargas@noaa.gov
--

# NOAA NESDIS STAR

ALGORITHM THEORETICAL BASIS DOCUMENT

Version: 1.0

Date: Feb. 2, 2018

TITLE: VIIRS VI Algorithm Theoretical Basis Document

Page 45 of 64

creator\_name = DOC/NOAA/NESDIS/STAR > VI Team, Center for Satellite Applications and Research, NESDIS, NOAA, U.S. Department of Commerce  
creator\_url = [https://www.star.nesdis.noaa.gov/smcd/viirs\\_vi/Monitor.htm](https://www.star.nesdis.noaa.gov/smcd/viirs_vi/Monitor.htm)  
date\_created = 2017-11-03T19:23:18Z  
geospatial\_bounds = POLYGON((-180.0 90.0, 180.0 90.0, 180.0 -90.0, -180.0 -90.0, -180.0 90.0))  
geospatial\_lat\_resolution = 0.036  
geospatial\_lat\_units = degrees\_north  
geospatial\_lon\_resolution = 0.036  
geospatial\_lon\_units = degrees\_east  
history = Created by VI algorithm v1.0  
id = 51bfbb25-4be3-42cf-8932-68b26acfd5f  
institution = DOC/NOAA/NESDIS/NDE > S-NPP Data Exploitation, NESDIS, NOAA, U.S. Department of Commerce  
instrument\_name = VIIRS  
naming\_authority = gov.noaa.nesdis.nde  
platform\_name = NPP  
process\_level = NOAA Level 3  
project = S-NPP Data Exploitation  
publisher\_email = [espcoperations@noaa.gov](mailto:espcoperations@noaa.gov)  
publisher\_name = DOC/NOAA/NESDIS/NDE > S-NPP Data Exploitation, NESDIS, NOAA, U.S. Department of Commerce  
publisher\_url = <http://projects.osd.noaa.gov/NDE>  
source = GITCO, JRR-AOD, JRR-CloudMask, SR, SVI01, SVI02  
standard\_name\_vocabulary = CF Standard Name Table (version 17, 24 March 2011)  
summary = TOA NDVI, TOC NDVI and TOC EVI in each pixel derived on a daily basis from VIIRS observations  
time\_coverage\_end = 2017-10-20T24:00:00Z  
time\_coverage\_start = 2017-10-20T00:00:00Z  
title = VIIRS\_VI

Conventions = CF-1.5  
Metadata\_Conventions = CF-1.5, Unidata Dataset Discovery v1.0  
cdm\_data\_type = grid  
creator\_email = [yunyue.yu@noaa.gov](mailto:yunyue.yu@noaa.gov)/[marco.vargas@noaa.gov](mailto:marco.vargas@noaa.gov)  
creator\_name = DOC/NOAA/NESDIS/STAR > VI Team, Center for Satellite Applications and Research, NESDIS, NOAA, U.S. Department of Commerce  
creator\_url = [https://www.star.nesdis.noaa.gov/smcd/viirs\\_vi/Monitor.htm](https://www.star.nesdis.noaa.gov/smcd/viirs_vi/Monitor.htm)  
date\_created = 2017-11-03T20:19:53Z  
geospatial\_bounds = POLYGON((130.0 90.0, 30.0 90.0, 30.0 -7.5, 130.0 -7.5, 130.0 90.0))  
geospatial\_lat\_resolution = 0.0090  
geospatial\_lat\_units = degrees\_north  
geospatial\_lon\_resolution = 0.0090

```
geospatial_lon_units = degrees_east
history = Created by VI algorithm v1.0
id = a43c72a3-1f14-4edf-8dbe-06b97a7bcb49
institution = DOC/NOAA/NESDIS/NDE > S-NPP Data Exploitation, NESDIS, NOAA,
U.S. Department of Commerce
instrument_name = VIIRS
naming_authority = gov.noaa.nesdis.nde
platform_name = NPP
process_level = NOAA Level 3
project = S-NPP Data Exploitation
publisher_email = espcoperations@noaa.gov
publisher_name = DOC/NOAA/NESDIS/NDE > S-NPP Data Exploitation, NESDIS,
NOAA, U.S. Department of Commerce
publisher_url = http://projects.osd.noaa.gov/NDE
source = GITCO, JRR-AOD, JRR-CloudMask, SR, SVI01, SVI02
standard_name_vocabulary = CF Standard Name Table (version 17, 24 March 2011)
summary = TOA NDVI, TOC NDVI and TOC EVI in each pixel derived on a daily
basis from VIIRS observations
time_coverage_end = 2017-10-20T24:00:00Z
time_coverage_start = 2017-10-20T00:00:00Z
title = VIIRS_VI
```

## ***3.5 Practical Considerations***

### **3.5.1 Numerical computation consideration**

The whole algorithm is composed of many straight forward calculations, thus, it is light computationally.

### **3.5.2 Programming and procedural consideration**

The VIIRS VI code runs every day with all the available SNPP input data for making the daily composites, daily rolling weekly and 16-day composites and produces the global and regional VI products.

### 3.5.3 Quality assessment and diagnostics

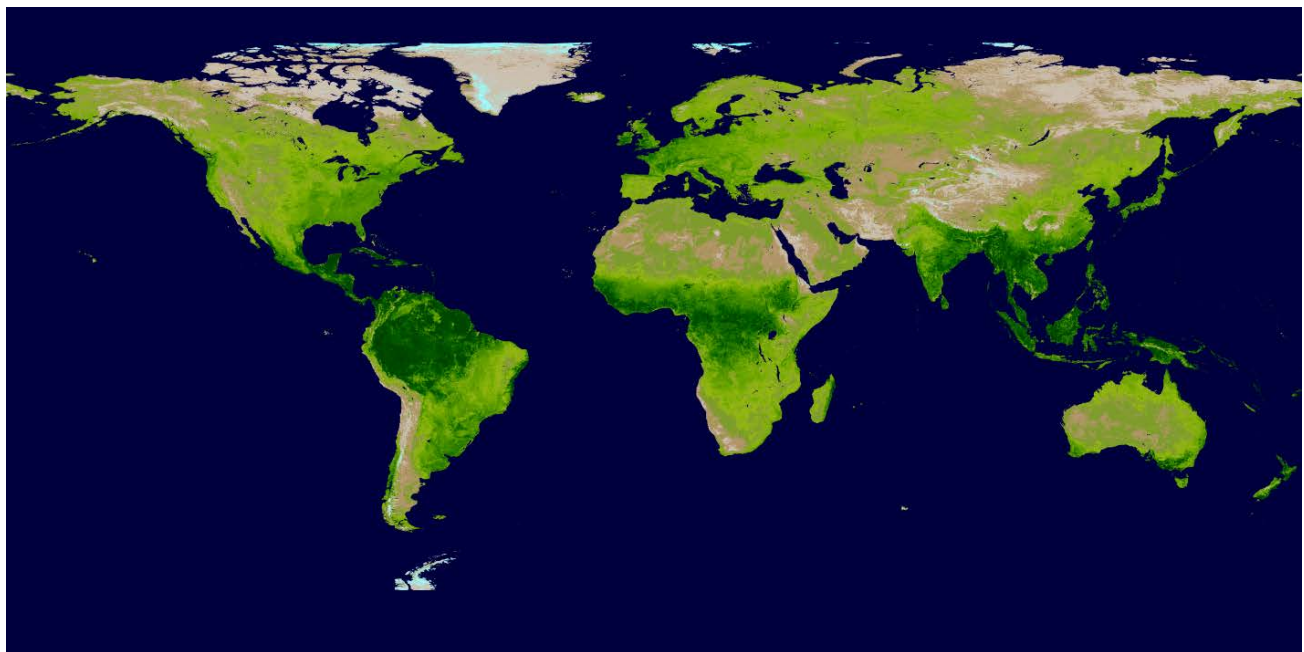
Unit testing and system testing include quality assessment of the VI products. Section 3.7 describes the validation of the VIIRS VI product with the MODIS VI products.

### 3.5.4 Exception handling

The expected exceptions, and a description of how they are identified, trapped, and handled, are provided in the system maintenance manual.

## 3.6 *Sample Results*

For visual examination of product quality, color-coded VI browse images in GeoTiff format for the global and regional VI products are shown in Fig. 9. The dimensions of the 0.036° resolution global VI browse image are 10000 and 5000. The dimensions of the 0.009° resolution regional VI browse image are 28889 and 10834.



(a)

# NOAA NESDIS STAR

ALGORITHM THEORETICAL BASIS DOCUMENT

Version: 1.0

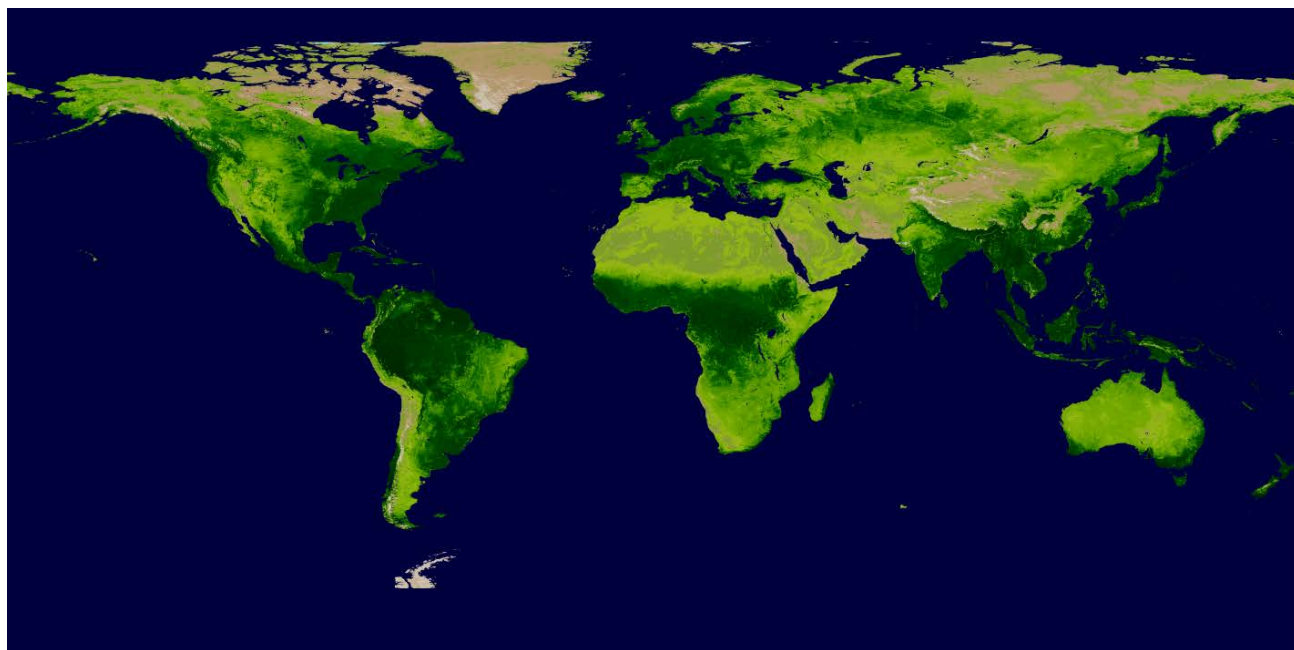
Date: Feb. 2, 2018

TITLE: VIIRS VI Algorithm Theoretical Basis Document

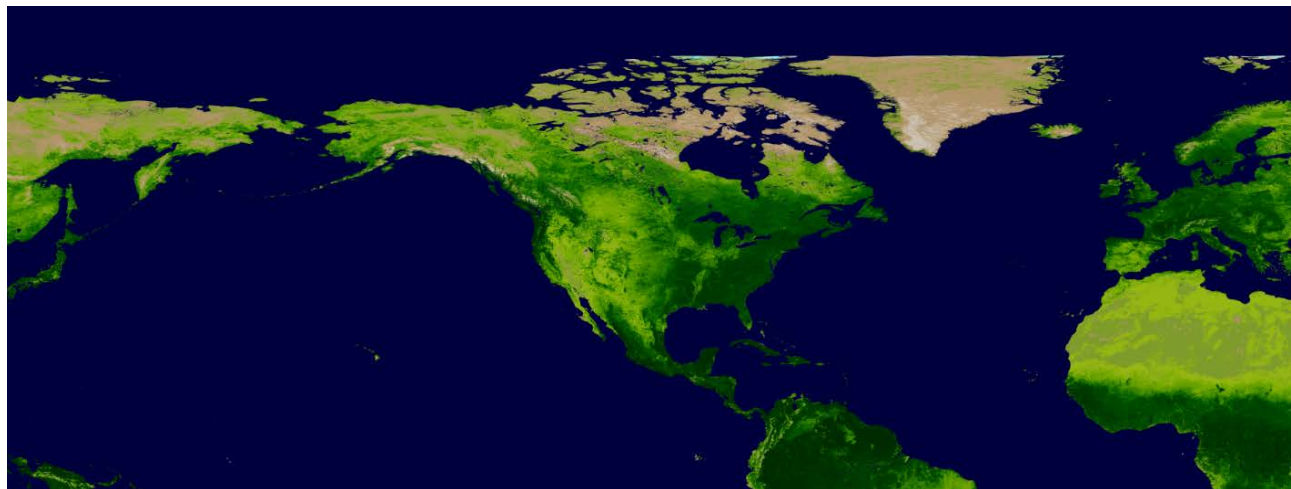
Page 48 of 64



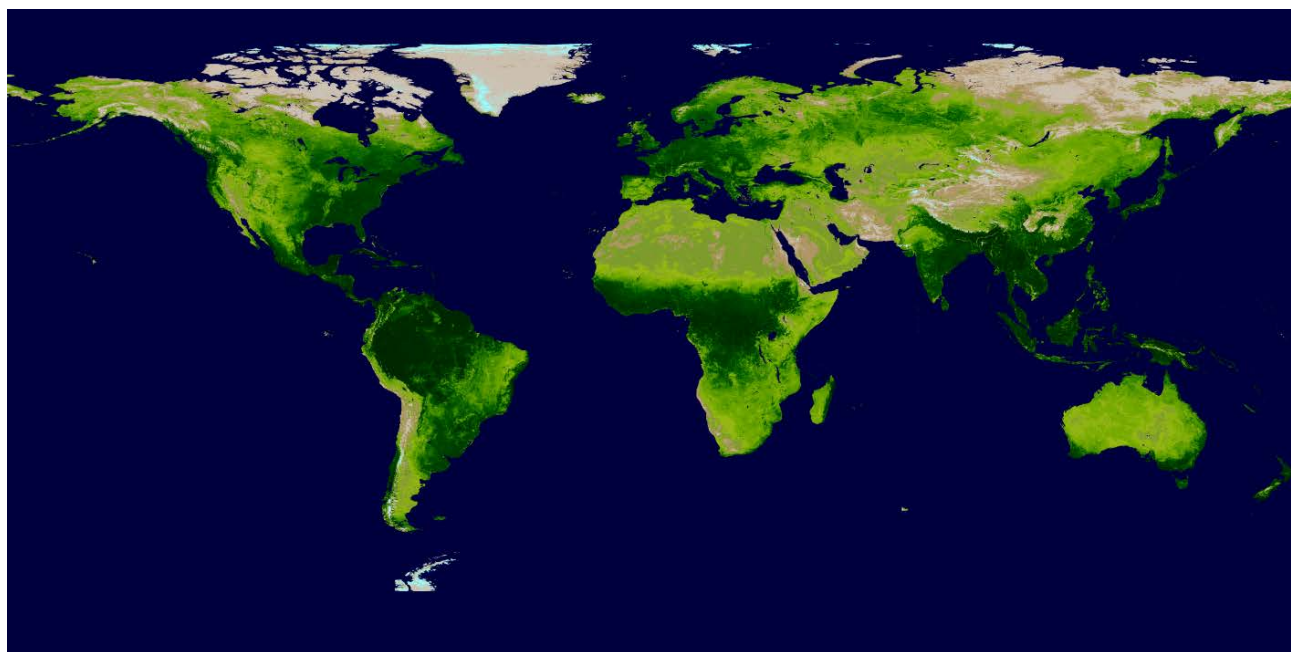
(b)



(c)



(d)



(e)

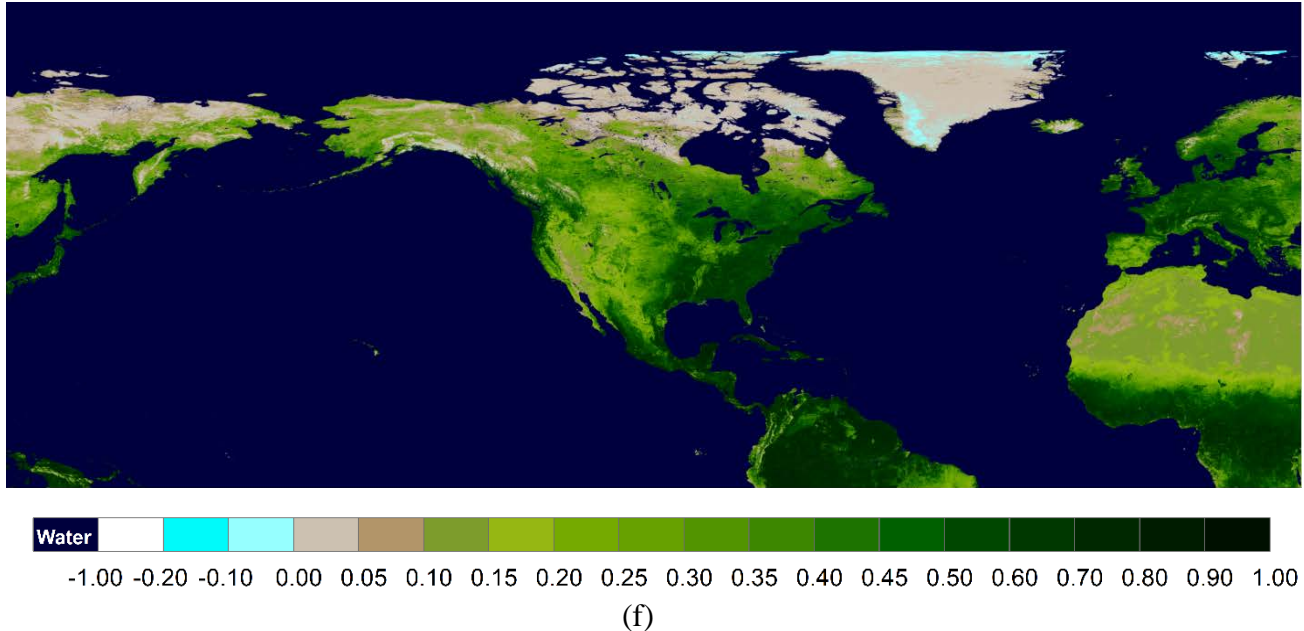


Figure 9. VIIRS VI browse images in the week of Oct 5-20, 2017. (a) VIIRS TOC global  $0.036^\circ$  16-day composite EVI; (b) VIIRS TOC regional  $0.009^\circ$  16-day composite EVI; (c) VIIRS TOA global  $0.036^\circ$  16-day composite NDVI; (d) VIIRS TOA regional  $0.009^\circ$  16-day composite NDVI; (e) VIIRS TOC global  $0.036^\circ$  16-day composite NDVI; (f) VIIRS TOC regional  $0.009^\circ$  16-day composite NDVI.

### 3.7 Validation Efforts

#### 3.7.1 Validation strategy

The VIIRS VI product validation process has started since 2013 when the S-NPP VIIRS was going to reach the provisional maturity stage in the IDPS system (Vargas et al., 2013). Results of the IDPS VIIRS data validation can be inherited in this NDE VIIRS VI product development since the product algorithm basically are the same. Additionally, the NDE VI products will be evaluated and validated by

- ▶ Product inter-comparison with other satellites (e.g., MODIS, AVHRR, Landsat, Planet etc.) over overlapping orbital tracks and over a globally-distributed set of sites;

- ▶ Time series comparison with in situ VI data and vegetation productivity (e.g., gross primary productivity) data over FLUXNET sites;
- ▶ Cross-comparison with AERONET-processed data.

VIIRS VI measurement accuracy, precision and uncertainty are calculated according to Eqs. 3.7-3.10. Accuracy is defined as the magnitude of the mean measurement error,

$$accuracy = |\mu| \quad (3.7)$$

where  $\mu$  is the mean measurement error.

$$\mu = \sum_{i=1}^n (VIIR\_VI_i - ref\_VI_i)^2 \quad (3.8)$$

Where  $ref\_VI$  is the reference VI to be compared with the VIIRS VI. Precision is defined as the standard deviation of the measurement errors.

$$Precision = \left[ \frac{1}{n-1} \sum_{i=1}^n (VIIR\_VI_i - ref\_VI_i - \mu)^2 \right]^{1/2} \quad (3.9)$$

Uncertainty is defined as the root mean square error (RMSE).

$$Uncertainty = \left[ \frac{1}{n} \sum_{i=1}^n (VIIR\_VI_i - ref\_VI_i)^2 \right]^{1/2} \quad (3.10)$$

### 3.7.2 Validation of VIIRS VI EDR granule product

The early version of the VIIRS VI EDR data are generated daily at the imagery resolution (375m at nadir) over land in swath/granule format (JPSS VVI ATBD, 2011). The data product ID for the VI EDR is VIVIO (VIIRS vegetation index operational product). An initial assessment of the SNPP VIIRS VI EDR was conducted by Marco, Miura, Shabanov and Kato (2013). In this assessment analysis, VIIRS, Aqua MODIS, and NOAA-18 AVHRR VI products over the period 2 May 2012 to 31 March 2013 were used. VIIRS Vegetation Index (VIVIO), Surface Reflectance (IVISR), and Geolocation (GIMGO) products in granule format were obtained and used to generate daily global gridded TOA NDVI and TOC EVI, and corresponding QF and geometry data sets. The MODIS data sources were Aqua MODIS 16-day TOC EVI (MYD13A2 Collection 5) in the gridded MODIS tile format (set of 1 km MODIS

Land tiles, sinusoidal projection), Aqua MODIS daily TOA reflectance (MYD02HKM Collection 5) in the swath format, and daily TOC reflectances (MYD09CMG Collection 5) in the Climate Modeling Grid (CMG) format (geographic projection, 0.05 degree). The daily MODIS data were processed into daily TOA NDVI and TOC EVI. Two types of analyses focused on an assessment of physical (global scale) and radiometric (regional scale) performances of VIIRS VI EDR.

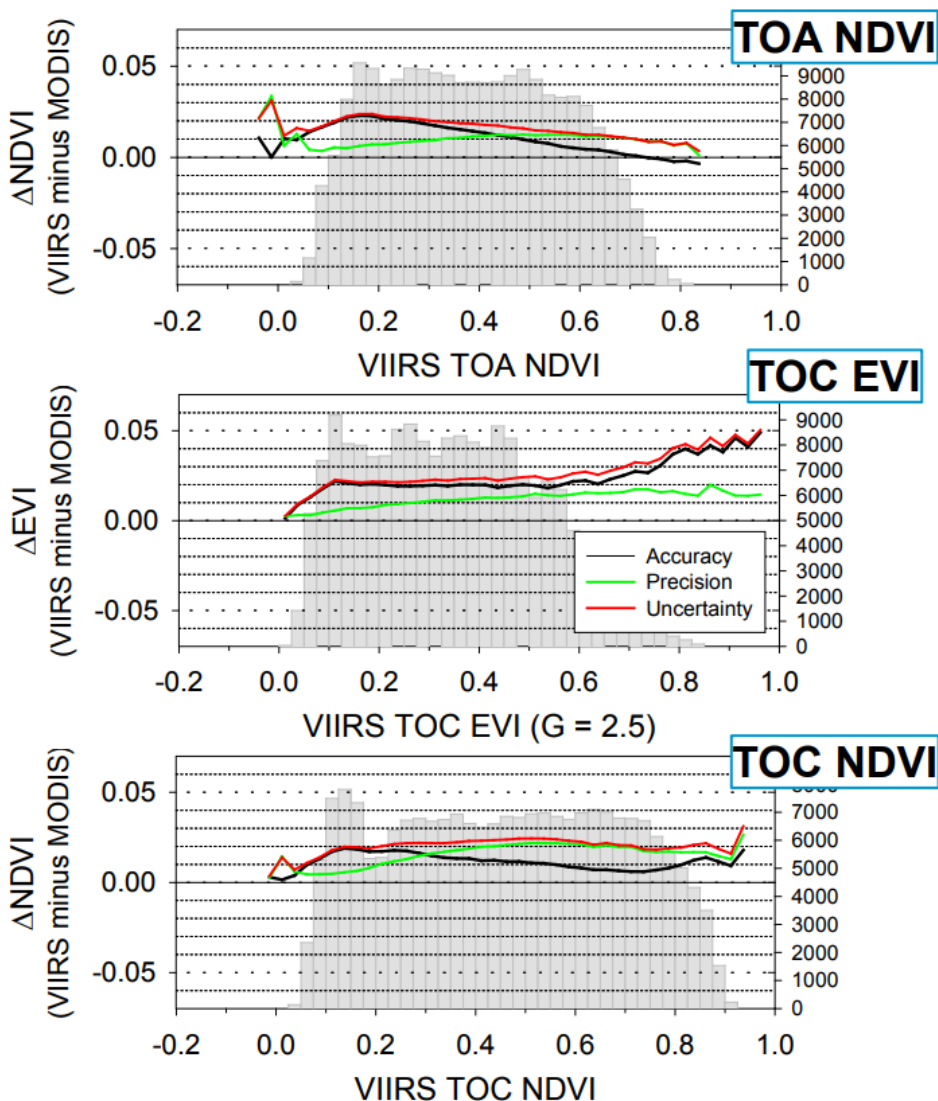
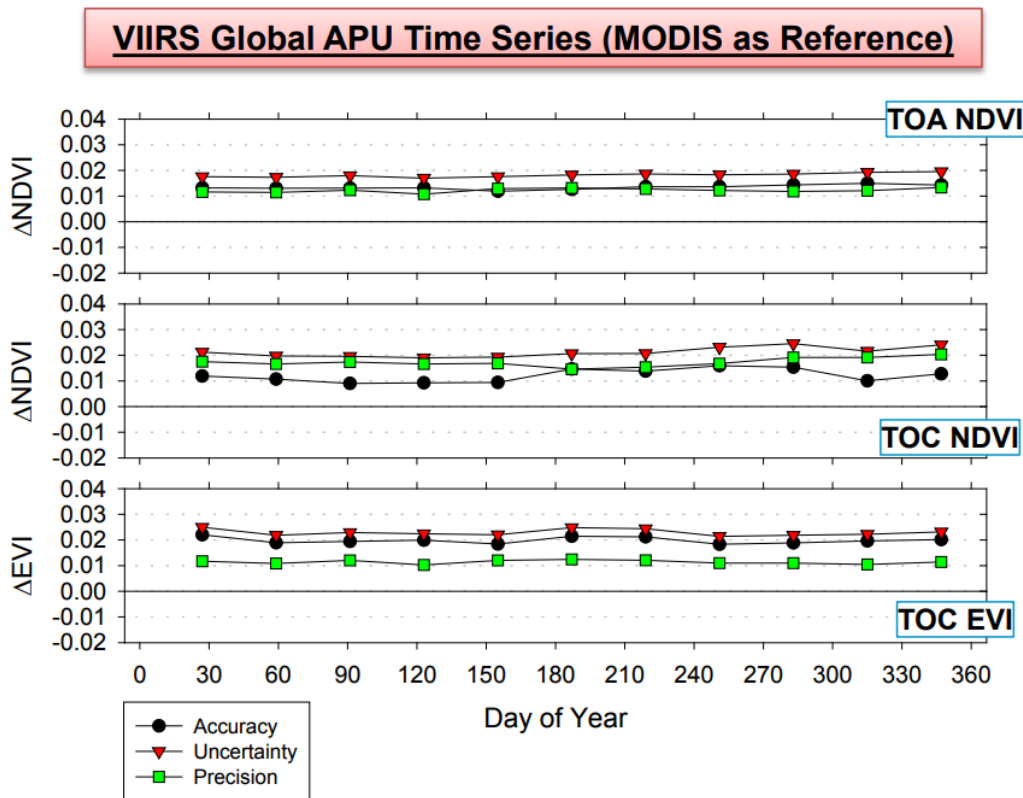


Figure 10. VIIRS TOA NDVI, TOC EVI and TOC NDVI Accuracy, Precision and Uncertainty (APU) are plotted as function of VIIRS VI values in global inter-comparison with MODIS VI.

The Accuracy, Precision and Uncertainty (APU) of VIIRS TOA NDVI, TOC NDVI and TOC EVI data were calculated using the counterpart VI calculated from the Aqua MODIS data as reference data. Fig.10 shows the APU of VIIRS VI as functions of VIIRS VI values. VIIRS TOA NDVI accuracy and uncertainty decreased with the increase of VI values, whereas the TOC EVI accuracy and uncertainty increased with the increase of VI values, particularly when EVI is larger than 0.7. TOC NDVI has relative stable APU with the increase of VI values.

Fig. 11 shows the APU time series of the VIIRS TOA NDVI, TOC NDVI and TOC EVI in global inter-comparison with the MODIS VI. TOA NDVI APU were stable and less than 0.02 in the whole year. TOC NDVI APU showed slightly seasonal variation. The uncertainty increased from DOY 250 to 280 and accuracy increased from DOY 180 to 280. TOC EVI accuracy and uncertainty also showed slightly seasonal variation with peaks at DOY 30 and DOY 180-220, whereas its precision is relative stable in the whole year.



*Figure 11. VIIRS TOA NDVI, TOC EVI and TOC NDVI Accuracy, Precision and Uncertainty (APU) time series in global inter-comparison with MODIS VI.*

The VIIRS VI EDR global APU are summarized in Table 16 (Marco et al, 2017). TOA NDVI has relatively small APU values, with an accuracy 0.013 NDVI unit, precision 0.012 and uncertainty 0.018. The accuracy and uncertainty of TOC NDVI were higher than those of TOA NDVI. The precision of TOC EVI was higher than those of TOA and TOC NDVI. Overall the VIIRS VI EDR met the Joint Polar Satellite System Program Level 1 Requirements Supplement (L1RDS) thresholds (U.S. Department of Commerce, 2014).

**Table 16. VIIRS VI EDR global APU estimation**

	TOA NDVI	TOC NDVI	TOC EVI	L1RDS threshold
Accuracy	0.013	0.020	0.012	0.05
Precision	0.012	0.011	0.018	0.04
Uncertainty	0.018	0.023	0.021	0.06

Miura, Muratsuchi and Vargas (2018) extended the assessment of VIIRS VI EDR granule product (Vargas et al. 2013) and cross-compared SNPP VIIRS VI EDR and MODIS VIs using near-coincident observation pairs obtained across the global for year 2015. In this VIIRS VI vs. MODIS VI comparison study, VIIRS and MODIS products were obtained in 3 days every month for the year 2015 when MODIS and VIIRS orbit tracts overlap. VIIRS VI EDR, daily TOA and surface reflectances, and geo-angle products were obtained from the Level-1 and Atmosphere Archive and Distribution System (LAADS) Distributed Active Archive Center (DAAC) (<https://ladsweb.modaps.eosdis.nasa.gov>). MODIS Collection 6 daily 500-m TOA and surface reflectance (MYD02HKM and MYD09, respectively), and geo-angle (MYD03) products were obtained from the LAADS DAAC.

As all of the unprojected VIIRS and MODIS granule data were first projected onto a geographic projection grid with nearest neighbor resampling and stitched into daily global mosaics. The grid sizes of 0.0036° by 0.004° and 0.004° by 0.004° were adopted for VIIRS and MODIS, respectively. Then the global mosaic data were spatially-aggregated into a coarser grid (0.036° by 0.040° or ~ 4 km), for meeting the JPSS VIIRS VI gridded product requirement. Miura, Muratsuchi and Vargas (2018) found that VIIRS VIs were slightly higher than the MODIS counterparts by 0.012-0.020 for the three VIs (see accuracy in Table 17). TOA NDVI and TOC NDVI cross-sensor differences were found not seasonally nor view zenith angle-dependent, whereas TOC EVI and TOC EVI2 cross-sensor differences found

were view zenith angle dependent where systematic differences increased with increasing view zenith angles (Miura et al. 2018). By band decomposition analysis, Miura et al. (2018) also found that NIR reflectance difference dominates the of VIIRS-MODIS cross-sensor TOA NDVI difference (which is small); while the TOC EVI difference is dominated by the observed view zenith angle differences.

Using the MODIS VI product as reference, the APU values of the VIIRS VI EDR were calculated and listed in Table 17. The VIIRS TOA NDVI has relative small uncertainty (0.018), and the TOC NDVI and EVI have a slightly higher uncertainty, 0.021 and 0.022, respectively. The VIIRS VI EDR met the Joint Polar Satellite System Program Level 1 Requirements Supplement (L1RDS) thresholds (U.S. Department of Commerce, 2014) again in this assessment.

**Table 17. VIIRS VI EDR global APU estimation in comparison with MODIS VIs**

	TOA NDVI	TOC NDVI	TOC EVI	L1RDS threshold
Accuracy	0.013	0.012	0.020	0.05
Precision	0.012	0.017	0.011	0.04
Uncertainty	0.018	0.021	0.022	0.06

### 3.7.3 Validation of VIIRS gridded and composited VI products

For validation of VIIRS gridded and composited VI products, only a preliminary validation can be performed since this is a new data development and only about two months of the NDE VIIRS VI data are available at current stage. A comprehensive validation over global coverage and long time series comparison analysis against the reference data (i.e., the *in situ* data and other satellite VI products) will be performed throughout the product calibration and validation phase.

#### 3.7.3.1 Validation data

The VI validation will be performed over 35 core flux tower sites defined by the EOS Land Product Validation Program [[http://landval.gsfc.nasa.gov/coresite\\_gen.html](http://landval.gsfc.nasa.gov/coresite_gen.html)). Among which 23 sites are in the U.S., 7 sites are in Eurasia, and 5 sites distributed in southern hemisphere. Fig. 10 shows geographic location of these FLUXNET sites. The sites represent a variety of land cover types including forest area, cropland, grassland and tundra.

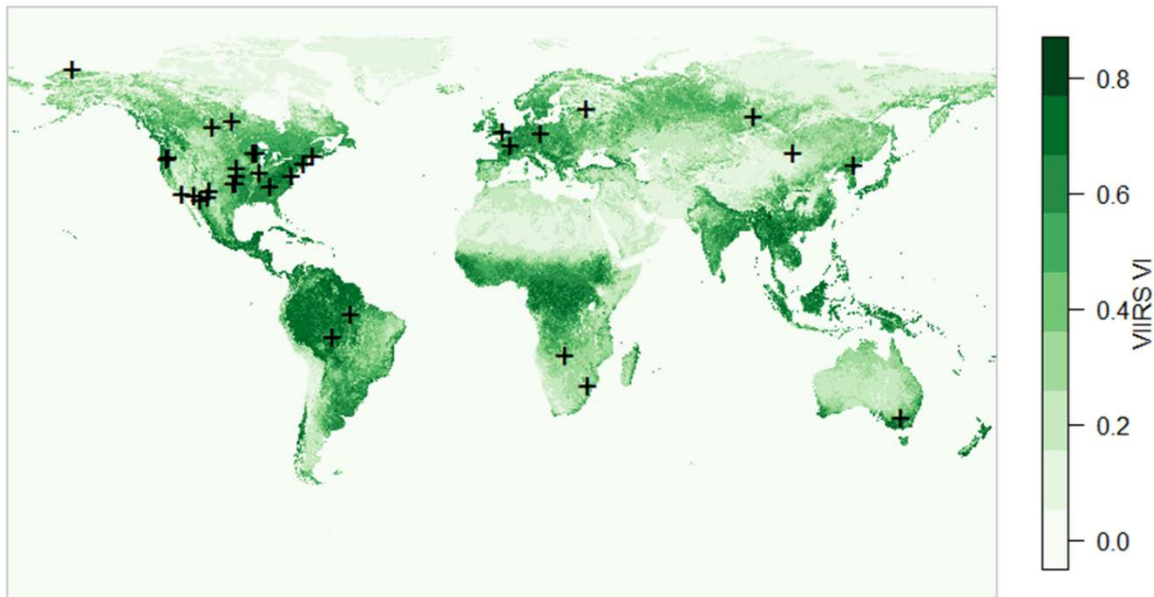


*Figure 12. The EOS Land Validation Core Sites of FLUXNET are intended as a focus for land product validation over a range of biome types.*

Biweekly NDE VIIRS VI data over the above sites, including the TOA NDVI, TOC EVI and the corresponding MODIS AQUA VI data (i.e., MYD13Q1), were extracted over those FLUXNET sites. In specific, the VIIRS VI data used are for the period October 14-November 19, 2017; the MODIS VI data are for the Julian day of 297 and 313. Note that 1) the NDE VIIRS VI data are available from October 2017, and 2) VIIRS VI biweekly products are daily rolling 16-day composite data. The FLUXNET tower VI data are not available due to about 6 months latency of the tower data release.

### 3.7.3.2 Comparison Results

The VIIRS VIs were compared to the MODIS VI data, shown in Fig. 11.

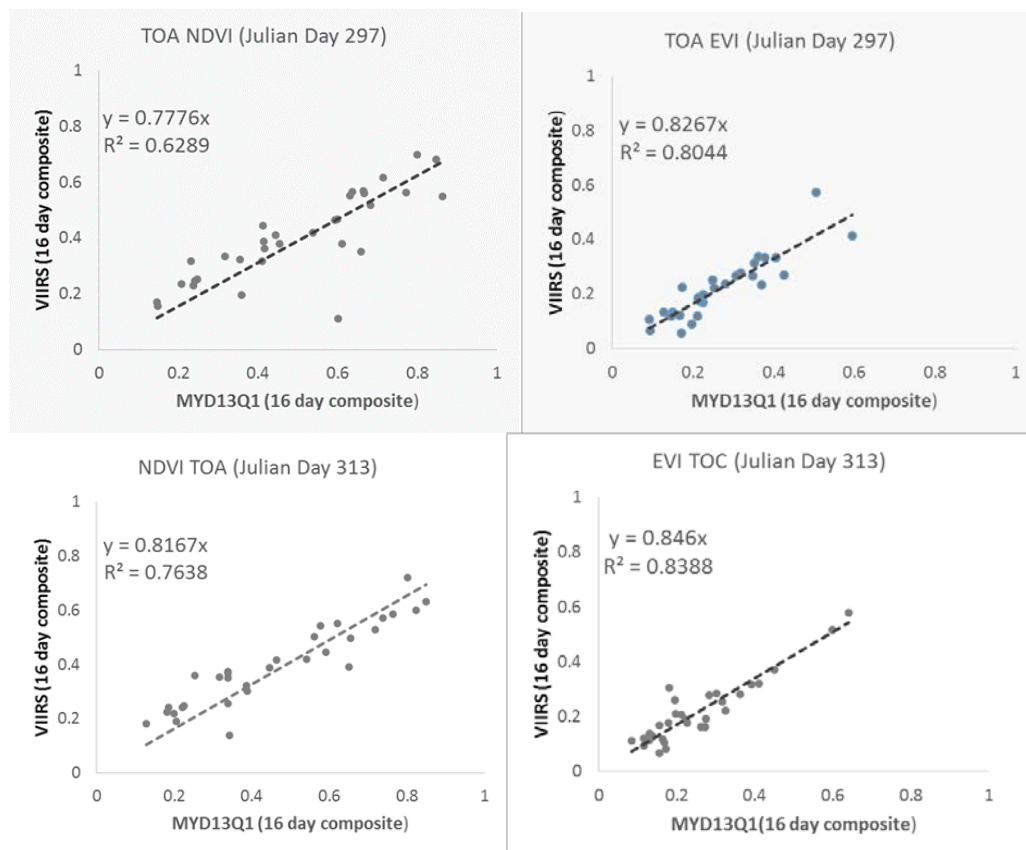


Figure 13. Scatterplots of the VIIRS and MODIS 16-day composite TOA NDVI data, over the 35 FLUXNET sites, on the Julian Day 297 (top-left) and Julian Day 313 (bottom-left), and the TOC EVI data on the Julian Day 313 (top-right) and Julian Day 313 (bottom-right).

Overall, the VIIRS biweekly VI products are comparable to the corresponding MODIS VI products, though there are some plots scattered away a little bit. To further investigate the site difference of the comparisons, a bar-chart figure are shown in Fig. 12. It indicates that comparison results from site to site may be different significantly. Further investigation on such differences will be performed in the product calibration and validation phase.

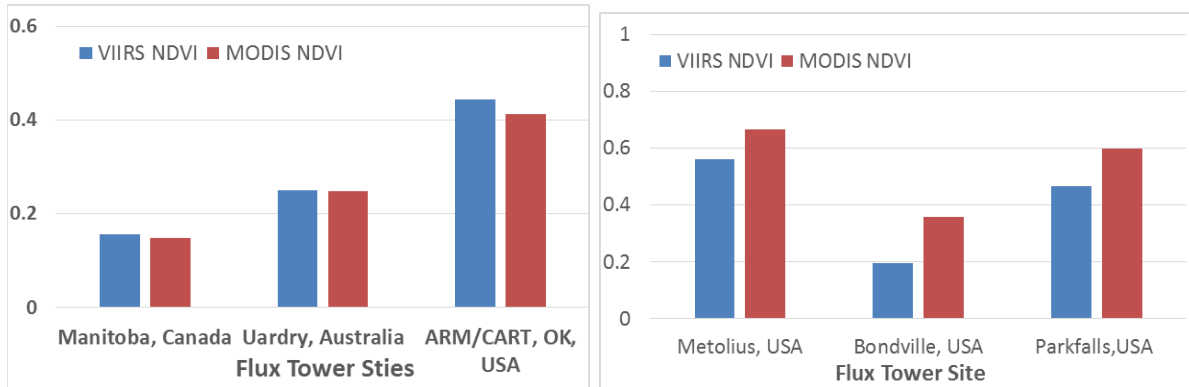


Figure 14. Bar-chart of the VIIRS and MODIS VI comparisons over 6 sample FLUXNET sites, in which the left 3 sites show great consistency of the two products (i.e. VIIRS VIs and MODIS VIs), while the right 3 sites show some obvious differences.

A simple statistics of the comparison results are computed and listed in Table 18, where

$$\text{Mean absolute error} = \frac{1}{n} \sum |VI_{VIIRS} - VI_{MODIS}| \quad (3.11)$$

$$\text{Accuracy} = \frac{1}{n} \sum (VI_{VIIRS} - VI_{MODIS}) \quad (3.12)$$

Where  $VI_{VIIRS}$  and  $VI_{MODIS}$  and VIIRS and MODIS NDVI or EVI values, respectively; n is the sample number. Again, overall, the statistics show a promise that the VIIRS VI products shall meet the requirements.

Table 18 summarize the comparison results in statistics.

**Table 18. VIIRS VI Validation Statistics**

	Mean absolute error	Accuracy
TOA NDVI	0.12	-0.04
TOC EVI	0.06	-0.02

In summary, preliminary results suggested that VIIRS VI observations are consistent with MODIS VI observations. Further evaluation will be conducted when MODIS global mosaic and flux tower VI measurements are available.

## 4. ASSUMPTIONS AND LIMITATIONS

### 4.1 *Assumptions*

The following assumptions have been made in determining that the VIIRS VI system architecture as designed will meet the requirements.

- VIIRS surface reflectance and TOA reflectance in I1, I2 and M3 bands are available, calibrated and navigated and are not distorted.
- JPSS Risk Reduction Unique Aerosol Optical Depth (JRR-AOD) data are available and the quality of the AOD data are high.
- JPSS Risk Reduction Unique Cloud Mask (JRR-CloudMask) data are available and the quality of the AOD data are high.

### 4.2 *Limitations*

The NVPS VIIRS VI system calculate vegetation index for all areas including snow and high latitude areas. But for the high latitude area in the North Hemisphere in winter, there is no optical observations from the VIIRS sensor due to the lack of sunlight or extremely high solar zenith angle ( $>80^\circ$ ). For pixels in this region, VI is missing.

There are large areas of cloud in the daily reflectance map. So the daily VI products are affected by the persistence of cloud.

The VIIRS NDVI and EVI data vary depending on the viewing and illumination geometry due to the bidirectional reflectance distribution function (BRDF) effects, particularly over the heterogeneous surface. There is no angular correction for the VIIRS NDVI and EVI data.

The variation of the atmospheric composition, such as aerosol, affects the quality of the TOA NDVI data. There is no atmospheric correction on the VIIRS TOA NDVI data.

## 5. LIST OF REFERENCES

- Ahl D. E., S. T. Gower, S. N. Burrows, N. V. Shabanow, R. B. Myneni, and Y. Knyazikhim (2006). Monitoring spring canopy phenology of a deciduous broadleaf forest using MODIS. *Remote Sensing of Environment*, 104, 88–95.
- Anyamba, A., and C. J. Tucker (2005). Analysis of Sahelian vegetation dynamics using NOAA-AVHRR NDVI data from 1981–2003. *Journal of Arid Environments*, 63, 596–614.
- Arvor, D., M. Jonathan, M. S. P. Meirelles, V. Dubreuil & L. Durieux (2011). Classification of MODIS EVI time series for crop mapping in the state of Mato Grosso, Brazil. *International Journal of Remote sensing*, 32, 7847–7871.
- Baret F., O. Hagolle, B. Geiger, P. Bicheron, B. Miras, M. Huc, B. Berthelot, F. Nino, M. Weiss, O. Samain, J. L. Roujean, and M. Leroy (2007). **Title of the paper?**, *Remote Sensing of Environment*, 110, 275–285.
- Blackburn, A. G. (1998), Quantifying chlorophylls and carotenoids at leaf and canopy scales: An evaluation of some hyperspectral approaches. *Remote Sensing of Environment*, 66, 273–285.
- Boegh, E., H. Soegaard, N. Broge, C. B. Hasager, N. O. Jensen, K. Schelde, K., **et al.** ?? (2002). Airborne multispectral data for quantifying leaf area index, nitrogen concentration, and photosynthetic efficiency in agriculture. *Remote Sensing of Environment*, 81, 179–193.
- Cabral, A., M. J. P. De Vasconcelos, J. M. C. Pereira, E. Bartholomé, and P. Mayaux (2003). Multi-temporal compositing approaches for SPOT-4 VEGETATION. *International Journal of Remote sensing*, 24 (16), 3343–3350.
- Carreiras, J.M B., J. M. C. Pereira, Y. E. Shimabukuro, and D. Stroppiana (2003). Evaluation of compositing algorithms over the Brazilian Amazon using SPOT-4 VEGETATION data. *International Journal of Remote sensing*, 24 (17), 3427–3440.
- Chen, J. M., and J. Cihlar (1996). Retrieving leaf area index of boreal conifer forests using Landsat TM images. *Remote Sensing of Environment*, 55, 153–162.
- Chen, X., L. Vierling, E. Rowell, and T. DeFelice (2004). Using lidar and effective LAI data to evaluate IKONOS and Landsat 7 ETM+ vegetation cover estimates in a ponderosa pine forest. *Remote Sensing of Environment*, 91, 14–26.

- Cihlar, J., D. Manak, and M. D'lorio (1994). Evaluation of compositing algorithms for AVHRR data over land. *IEEE Transactions on Geoscience and Remote Sensing*, 32 (2), 427-437.
- Defries, R. S., and A. S. Belward, (2000). Global and regional land cover characterization from satellite data. *International Journal of Remote Sensing*, 21, 1083-1092.
- Di Bella, C. M., Paruelo, J. M., Becerra, J. E., Bacour, C., & Baret, F. (2004). Effect of senescent leaves on NDVI-based estimates of f APAR: experimental and modelling evidences. *International Journal of Remote Sensing*, 25, 5415-5427.
- Funk, C. and M. E. Budde (2009). Phenologically-tuned MODIS NDVI-based production anomaly estimates for Zimbabwe. *Remote Sensing of Environment*, 113, 115-125.
- Gitelson, A. A., Vina, A., Ciganda, V., Rundquist, C. D., & Arkebauer, J. T. (2005). Remote estimation of canopy chlorophyll content in crops. *Geophysical Research Letters*, 32, L08403. doi:10.1029/2005GL022688.
- Gutman, G. (1991). Vegetation indices from AVHRR: an update and future prospects. *Remote Sensing of Environment*, 35, 121-136.
- Gutman, G., and A. Ignatov (1998). The derivation of the green vegetation fraction from NOAA/AVHRR data for use in numerical weather prediction models. *International Journal of Remote Sensing* 19, 1533-1543.
- Holben, B. (1986). Characteristics of maximum-value composite images from temporal AVHRR data. *International Journal of Remote Sensing*, 7, 1417-1434.
- Houborg, R., H. Soegaard, and E. Boegh (2007). Combining vegetation index and model inversion methods for the extraction of key vegetation biophysical parameters using Terra and Aqua MODIS reflectance data. *Remote Sensing of Environment*, 106, 39-58.
- Huete, A. R. (1988). A soil-adjusted vegetation index (SAVI). *Remote Sensing of Environment*, 25, 295-309.
- Huete, A. R., G. Hua, J. Qi, A. Chehbouni, and W. J. D. van Leeuwn (1992). Normalization of multidirectional red and NIR reflectances with the SAVI. *Remote Sensing of Environment*, 41, 143-154.
- Huete, A. R., K. Didan, T. Miura, E. P. Rodriguez, X. Gao, and L. G. Ferreira (2002). Overview of the radiometric and biophysical performance of the MODIS vegetation indices. *Remote Sensing of Environment*, 83, 195-213.

- Huete, A. R., K. Didan, Y. E. Shimabukuro, P. Ratana, C. R. Saleska, L. R. Hutya, W. Yang, R. R. Nemani, and R. Myneni, (2006). Amazon rainforests green-up with sunlight in dry season. *Geophysical Research Letters*, 33, L06405, doi:10.1029/2005GL025583.
- Jiang, Z., A. R. Huete, J. Chen, Y. Chen, J. Li, G. Yan, and X. Zhang (2006). Analysis of NDVI and scaled difference vegetation index retrievals of vegetation fraction. *Remote Sensing of Environment*, 101, 366-378.
- Jiang, Z., A.R. Huete, K. Didan, T. Miura (2008). Development of a two-band enhanced vegetation index without a blue band. *Remote Sensing of Environment*, 112, 3833–3845.
- Joint Polar Satellite System (JPSS) VIIRS Vegetation Index (VVI) Algorithm Theoretical Basis Document (ATBD), April 22, (2011).
- Kaufman, Y. J., and D. Tanré (1992). Atmospherically resistant vegetation index (ARVI) for EOS-MODIS. *IEEE Transactions on Geoscience and Remote Sensing*, 30, 261-270.
- Liu, H., and A. R. Huete (1995). A feedback based modification of the NDVI to minimize canopy background and atmospheric noise. *IEEE Transactions on Geoscience and Remote Sensing*, 33, 457-465.
- Lunetta, R. S., J. F. Knight, J. Ediriwickrema, J. G. Lyon, and L. D. Worthy (2006). Land-cover change detection using multi-temporal MODIS NDVI data. *Remote Sensing of Environment*, 105, 142-154.
- Miura, T., J. Muratsuchi, and M. Vargas. (2018). Cross-comparison of VIIRS and MODIS vegetation indices using one-year global data. *Remote Sensing*, (in preparation).
- Myneni, B. R., Keeling, D. C., Tucker, J. C., Asrar, G., & Nemani, R. R. (1997a). Increased plant growth in the northern high latitudes from 1981 to 1991. *Nature*, 386(17), 698–702.
- Myneni, B. R., Nemani, R. R., & Running, W. S. (1997b). Estimation of global leaf area and absorbed PAR using radiative transfer models. *IEEE Transactions on Geoscience and Remote Sensing*, 35, 1380–1393.
- Nagler, P. L., Cleverly, J., Glenn, E., Lampkin, D., Huete, A. R., & Wan, Z. (2005). Predicting riparian evapotranspiration from MODIS vegetation indices and meteorological data. *Remote Sensing of Environment*, 94, 17–30.
- Rahman, A. F., D. A. Sims, V. D. Cordova, and B. Z. El-Masri (2005). Potential of MODIS EVI and surface temperature for directly estimating per-pixel ecosystem C fluxes. *Geophysical Research Letters*, 32, L19404, doi:10.1029/2005GL024127.

- Sims, D. A., A. F. Rahman, V. D. Cordova, B. Z. El-Masri, D. D. Baldocchi, L. B. Flanagan, A. H. Goldstein, D. Y. Hollinger, L. Misson, R. K. Monson, W. C. Oechel, H. P. Schmid, S. C. Wofsy, and L. Xu (2006). On the use of MODIS EVI to assess gross primary productivity of North American ecosystems. *Journal of Geophysical Research*, 111, G04015, doi:10.1029/2006JG000162.
- Sims, D. A., Rahman, A. F., Cordova, V. D., El-Masri, B. Z., Baldocchi, D. D., Bolstad, P. V., et al. (2008). A new model of gross primary productivity for North American ecosystems based solely on the enhanced vegetation index and land surface temperature from MODIS. *Remote Sensing of Environment*, 112, 1633–1646.
- Stoms, D.M., Bueno, M.J., Davis, F.W. (1997). Viewing geometry of AVHRR image composites derived using multiple criteria. *Photogrammetric Engineering & Remote Sensing*, 63 (6), 681-689.
- Suzuki, K., Masuda, K., & Dye, D. G. (2007). Interannual covariability between actual evapotranspiration and PAL and GIMMS NDVIs of northern Asia. *Remote Sensing of Environment*, 106, 387–398.
- Townshend, J. R. G. (1994). Global data sets for land applications from the advanced very high resolution radiometer: An introduction. *International Journal of Remote Sensing*, 15, 3319–3332.
- Tucker, J. C., Fung, I. Y., Keeling, C. D., & Gammon, R. H. (1986). Relationship between atmospheric CO<sub>2</sub> variations and a satellite-derived vegetation index. *Nature*, 319, 195–199.
- U.S. Department of Commerce. (2014). Joint Polar Satellite System Program Level 1 Requirements Supplement (Version 2.10). Retrieved from [http://www.jpss.noaa.gov/assets/pdfs/technical\\_documents/level\\_1\\_requirements\\_supplement.pdf](http://www.jpss.noaa.gov/assets/pdfs/technical_documents/level_1_requirements_supplement.pdf)
- van Leeuwen, W.J.D., Huete, A.R., Laing, T.W. (1999). MODIS vegetation index compositing approach: a prototype with AVHRR data. *Remote Sensing of Environment*, 69 (3), 264-280.
- Vargas, M., Miura, T., Shabanov, N., & Kato, A. (2013). An initial assessment of Suomi NPP VIIRS vegetation index EDR. *Journal of Geophysical Research-Atmospheres*, 118, 12301-12316.
- Vargas, M., T. Miura, Z. Jiang, M. Chen, A. Kato, J. Muratsuchi. (2017). NOAA SNPP/JPSS VIIRS vegetation products and algorithm development. 97<sup>th</sup> AMS Annual Meeting, 22-26 January 2017, Seattle, WA.

- Wardlow, B. D., Egbert, S. L., & Kastens, J. H. (2007). Analysis of time-series MODIS 250m vegetation index data for crop classification in the U.S. Central Great Plains. *Remote Sensing of Environment*, 108, 290–310.
- Waring, R. H., Coops, N. C., Fan, W., & Nightingale, J. M. (2006). MODIS enhanced vegetation index predicts tree species richness across forested ecoregions in the contiguous U.S.A. *Remote Sensing of Environment*, 103, 218–226.
- Wessels, K. J., S. D. Prince, P. E. Frost, and D. van Zyl (2004). Assessing the effects of human-induced land degradation in the former homelands of northern South Africa with a 1 km AVHRR NDVI time-series. *Remote Sensing of Environment*, 91, 47-67.
- Xiao, X., Hagen, S., Zhang, Q., Keller, M., & Moore, B. (2006). Detecting leaf phenology of seasonally moist tropical forests in South America with multi-temporal MODIS images. *Remote Sensing of Environment*, 103, 465–473.
- Xiao, X., Hollinger, D., Aber, J., Goltz, M., Davidson, E. A., Zhang, Q., et al. (2004). Satellitebased modeling of gross primary production in an evergreen needleleaf forest. *Remote Sensing of Environment*, 89, 519–534.
- Zeng, X., Dichinson, E. R., Walker, A., & Shaikh, M. (2000). Derivation and evaluation of global 1-km fractional vegetation cover data for land modeling. *Journal of Applied Meteorology*, 39, 826–839.
- Zhang, X., A. F. Mark, B. S. Crystal, H. S. Alan, C. F. H. John, F. Gao, C. R. Bradley and A. Huete. (2003). *Remote Sensing of Environment*, 84, 471-475.